

CONFIDENTIAL

Copy ^{C2} ^A
RM E58D17

NACA RM E58D17

UNCLASSIFIED



RESEARCH MEMORANDUM

DESIGN AND EXPERIMENTAL PERFORMANCE OF A 0.35 HUB-TIP
RADIUS RATIO TRANSONIC AXIAL-FLOW-COMPRESSOR ROTOR

DESIGNED FOR 40 POUNDS PER SECOND

PER UNIT FRONTAL AREA

By John C. Montgomery and Paul T. Yasaki

Lewis Flight Propulsion Laboratory
Cleveland, Ohio

LIBRARY COPY

SEP 5 1958

LANGLEY AERONAUTICAL LABORATORY
LIBRARY, NACA
LANGLEY FIELD, VIRGINIA

CLASSIFIED DOCUMENT

This material contains information affecting the National Defense of the United States within the meaning of the espionage laws, Title 18, U.S.C., Secs. 793 and 794, the transmission or revelation of which in any manner to an unauthorized person is prohibited by law.

NATIONAL ADVISORY COMMITTEE FOR AERONAUTICS

WASHINGTON

September 4, 1958

CLASSIFICATION CHANGED

UNCLASSIFIED

By ^{FB} ⁰⁹⁻⁸⁸⁻⁶⁰ ⁷⁻²⁸⁻⁶⁰ ^{Date}
1pa # 27

CONFIDENTIAL

UNCLASSIFIED

CONFIDENTIAL

UNCLASSIFIED

NATIONAL ADVISORY COMMITTEE FOR AERONAUTICS

RESEARCH MEMORANDUM

DESIGN AND EXPERIMENTAL PERFORMANCE OF A 0.35 HUB-TIP RADIUS

RATIO TRANSONIC AXIAL-FLOW-COMPRESSOR ROTOR

DESIGNED FOR 40 POUNDS PER SECOND

PER UNIT FRONTAL AREA*

By John C. Montgomery and Paul T. Yasaki

SUMMARY

An investigation was conducted to determine the feasibility of a high-performance transonic axial-flow-compressor stage with a weight flow of 40 pounds per second per square foot of frontal area. A transonic axial-flow inlet stage with a hub-tip ratio of 0.35 and an axial Mach number of approximately 0.75 was designed and fabricated. The design employed constant energy addition (vortex type) at all radii through the rotor. No guide vanes were used, and inlet air was assumed axial. Double-circular-arc blades with leading- and trailing-edge radii of 0.010 inch were employed. The rotor was designed to produce a total-pressure ratio of 1.51 at an equivalent specific weight flow of 40 pounds per second per square foot of frontal area. This report presents the rotor design method, plus rotor over-all performance, and blade-element data.

At the design equivalent tip speed of 1100 feet per second, a peak rotor adiabatic efficiency of 89 percent was obtained at an equivalent specific weight flow of 38.0 pounds per second per square foot of frontal area with an average total-pressure ratio of 1.51. Peak efficiencies of 0.98, 0.98, 0.96, 0.93, and 0.84 were obtained at 60, 70, 80, 90, and 110 percent of design speed, respectively.

The method employed for computing the velocity distribution was good for the rotor inlet but was not sufficient for the rotor outlet, where the losses were underestimated. The radial matching of the blade-element parameters was good, however, at a flow of 38.34 pounds per second per square foot. Therefore, good compressor efficiency was obtained at a weight flow below the design value. The high losses obtained at the rotor tip section were shown to be primarily a function of shock losses.

* Title, Confidential.

CONFIDENTIAL

UNCLASSIFIED

INTRODUCTION

Previous investigations (refs. 1 to 4) have pointed out the numerous advantages of transonic inlet stages in axial-flow compressors. In each of these studies, a transonic axial-flow rotor was designed, fabricated, and tested to advance the science of designing transonic stages for a wide range of flow conditions. Experimental investigations (refs. 3 to 5) have shown that weight flow per unit frontal area can be improved without sacrificing efficiency or stage pressure ratio by decreasing the hub-tip radius ratio and increasing the inlet axial Mach number. In the work of reference 6 a weight flow of 35.6 pounds per second per unit frontal area was obtained with rotor having a 0.4 hub-tip radius ratio at a total-pressure ratio of 1.38 and an efficiency of 0.91.

In this investigation the hub-tip radius ratio was further decreased to 0.35 and the design average inlet axial Mach number was increased to approximately 0.75 in order to attain a design weight flow of 40 pounds per square foot of frontal area. Guide vanes were not used, and inlet air was assumed axial. The rotor design tip diffusion factor was limited to approximately 0.35; this in conjunction with a tip speed of 1100 feet per second resulted in a design over-all total-pressure ratio of 1.51.

The over-all performance and the blade-element performance of the rotor as obtained from detailed instrument surveys are presented herein. The rotor blade-element data are presented for corrected tip speeds of 770, 990, 1100, and 1210 feet per second.

COMPRESSOR DESIGN

Velocity Diagram Calculations

In the design of the compressor inlet stage reported herein the following conditions were selected:

- (1) Hub-tip diameter ratio of 0.35 at the rotor inlet with an inlet tip diameter of 14 inches
- (2) Specific weight flow of 40 pounds per second per square foot with blockage factors at the rotor inlet and rotor outlet of 0.98 and 0.97, respectively
- (3) Inlet tip speed of 1100 feet per second
- (4) Rotor chord of 2 inches and tip solidity of approximately 1.0
- (5) Tip taper across the rotor

- (6) Rotor tip diffusion factor of approximately 0.35
- (7) Average axial-velocity ratio of 1.0 across the rotor
- (8) Radially constant energy addition
- (9) No inlet whirl
- (10) Radially constant value of the blade-element total-pressure-loss coefficient

Tip taper across the rotor was specified so that the rotor hub cone angle could be held within conventional limits and so that outer-wall curvature could be utilized to increase the axial-velocity ratio across the rotor tip section. Reference 5 indicates that an increase in the axial-velocity ratio across the rotor tip section is desirable. The total-pressure-loss coefficient ω was selected as 0.025 to correspond to a mean passage value.

Preliminary calculations for the rotor were made with the above conditions assuming various degrees of tip taper and assuming constant axial velocity across the passage. The results indicate that a tip taper ratio $r_{t,2}/r_{t,1}$ of 0.97 would result in an acceptable hub cone angle of approximately 20° and a rotor hub absolute outlet Mach number of slightly less than 1.0. (Symbols are defined in appendix A.)

Using a tip taper ratio of 0.97, calculations were made along conical surfaces to determine the required rotor outlet hub radius assuming constant axial-velocity distributions before and after the rotor. In the calculations the area at each axial station was corrected for the assumed boundary-layer blockage factors (0.98 at the inlet and 0.97 at the outlet). The rotor outlet hub radius was therefore fixed before any corrections were made to the assumption of constant axial-velocity distribution.

Fairing of the annulus contours on both the inner and the outer walls was done by use of circular arcs and straight lines as much as possible in order to simplify the calculations required to determine the effect of wall curvature on the radial distribution of the axial velocity across the blade passage. The effect of wall curvature on the axial-velocity distribution before and after the rotor was calculated by a procedure similar to that outlined in reference 7. The procedure of reference 7 was modified slightly inasmuch as the derivatives of the streamlines were determined analytically. In order to determine the derivatives (curvature) of the streamlines, the streamlines were assumed to be surfaces of revolution which divide the annulus area into ten equal increments. The surfaces of revolution were assumed to be continuous and to extend beyond both the upstream and the downstream axial measuring

4713

CA-1 back

stations. The radius of a surface of revolution at any given axial location was assumed as $r = \sqrt{r_t^2 - k(r_t^2 - r_h^2)}$, where k is the desired percent of area between the outer wall and the given surface of revolution. Varying k from 0 to 1.0 gives the radius of the eleven surfaces of revolution (ten equal-area increments) at a given axial location. When $k = 0$ the radius of the outer wall is obtained; when $k = 1.0$ the radius of the inner wall is obtained; when k is between 0 and 1.0 the radii of the assumed surfaces of revolution are obtained. On the inner and outer surfaces of revolution (inner and outer walls) the values of r_h and r_t are not constant and vary along the axial direction. Therefore, the equation of the radii of the surfaces of revolution may be differentiated with respect to the axial direction to obtain the derivatives of the assumed surfaces of revolution. The derivatives of the assumed surfaces of revolution were, therefore, obtained at a given axial location as a function of the geometry (inner- and outer-wall radii, surface of revolution, radius, and inner- and outer-wall derivatives) at the same axial location. The derivatives thus obtained were used in the procedure outlined in reference 7 to calculate the distribution of the axial velocity before and after the rotor.

The calculations for the axial-velocity distribution at the rotor outlet for the given rotor design were made by using a vortex tangential velocity distribution ($V_\theta = K/r$) and assuming no radial gradient of entropy.

With the corrected axial-velocity distribution it was necessary to alter the blade loading slightly so that the design value of the diffusion factor at the rotor tip would still be approximately 0.35. Based on the previous assumptions, the design value of the mass-averaged total-pressure ratio was 1.51.

Blade Selection

After the design velocity diagrams were determined, the blade sections which would produce the desired velocity diagrams were selected.

Double-circular-arc blades with leading- and trailing-edge radii of 0.010 inch were employed. From strength considerations, the maximum thickness ratio of the rotor was selected to vary from 8 percent of chord at the hub to 5 percent at the tip.

The design rules of reference 8 were used to determine the incidence angle, deviation angle, and camber angle for each rotor blade section. Since the blade setting and camber angles of the rotor hub section were beyond the realm of the rotors used to formulate the design rules of reference 8, a check was made to determine whether choking would occur

before the selected optimum incidence angles were reached. The choking analysis of reference 9, which was used to check the selected values of optimum incidence angle, indicated that choking would not occur.

The resultant values of the rotor blade design configuration and geometry are presented in table I for the blade sections located along conical surfaces at 10, 30, 50, 70, and 90 percent of the passage height from the outer wall.

Rotor Outlet Annulus

In order to prevent choking in the annulus during tests of the rotor alone, the annulus area downstream of the rotor outlet measuring station was enlarged (fig. 1(a)). This increase in passage flow area was accomplished by continuing both the hub and tip wall curvatures as far as permissible. In this manner the effect of enlarging the outlet passage minimized the possibility of affecting the design axial-velocity distribution after the rotor.

APPARATUS AND PROCEDURE

Compressor Installation

The compressor installation is shown in the schematic diagram of figure 1(b). Air is drawn in through a submerged sharp-edged thin-plate orifice and an air-operated butterfly valve into a 72-inch-diameter inlet depression tank. A series of screens is located approximately 60 inches upstream of the compressor inlet bellmouth to provide a smooth and uniform flow at the inlet. The compressor outlet air passes into an annular collector and into the laboratory altitude exhaust system. An electrically operated gate valve installed in the exhaust line is operated in conjunction with the inlet valve to adjust the compressor weight flow and inlet pressure.

Power for the compressor is supplied by a 1500-horsepower induction motor through a speed-increasing gearbox. Compressor speed was controlled by varying the frequency supplied to the alternating-current motor.

Instrumentation

Airflow through the compressor was measured by means of a sharp-edged thin-plate orifice and by survey instrumentation at the rotor inlet. Pressure drop across the orifice was measured on a water manometer, and the orifice temperature was measured by iron-constantan thermocouples.

Inlet tank temperature and pressure were measured approximately 21 inches upstream of the compressor inlet bellmouth by averaging the readings from five iron-constantan thermocouple probes and five wall static-pressure taps around the circumference of the tank. The thermocouple probes were located to make measurements at the center of equal annulus areas.

The axial stations used to measure the rotor performance are shown in figure 1(a). Station 1 is located 1/2 inch upstream of the rotor blade hub leading edge, and station 2 is located 1/2 inch downstream of the hub trailing edge. At the rotor inlet (station 1), total pressure, air angle, and static pressure were measured. All measurements were taken at the five major radial positions (10, 30, 50, 70, and 90 percent of the passage height from the outer wall); in addition, total pressure and air angle were measured at 3, 5, 7, 93, 95, and 97 percent of the passage height from the outer wall.

At the rotor outlet (station 2), total pressure, total temperature, air angle, and static pressure were measured. Static pressures were measured at the five major radial positions and at the inner and outer walls. Total pressure, total temperature, and air angle were measured and recorded continually by an automatic recorder as an instrument probe traversed the passage radially.

Wall static-pressure taps were installed at each axial measuring station on both the inner and the outer walls. In addition, ten static-pressure taps were installed axially at 1/4-inch intervals between stations 1 and 2 along the outer wall.

A magnetic blade vibration pickup was mounted in the compressor casing near the rotor blade leading edge. This pickup was used to give a qualitative indication of the blade tip vibration.

Procedure

Over-all and blade-element performance data points were taken at 60, 70, 80, 90, 100, and 110 percent of design speed. Inlet pressure was maintained at 20 inches of mercury for all speeds. Weight flow was varied from the maximum obtainable to a value where blade vibrations were encountered, or to a point where the blade tip adiabatic efficiency dropped to approximately 70 percent.

Equations used for the solutions of various parameters are given in appendix B.

RESULTS AND DISCUSSION

Over-All Rotor Performance

The over-all performance of the rotor is presented in figure 2 as a plot of mass-averaged total-pressure ratio and mass-averaged efficiency against corrected specific weight flow measured at the rotor inlet. The over-all performance is presented for the corrected tip speeds of 660, 770, 880, 990, 1100, and 1210 feet per second (corresponding to 60, 70, 80, 90, 100, and 110 percent of design speed).

At design speed (1100 ft/sec) the rotor produced the design pressure ratio of 1.51 at a specific weight flow of 38.0 pounds per second per square foot and an efficiency of 0.89. Since the rotor was designed for a weight flow of 40 pounds per second per square foot, the weight flow was low by 5 percent. Maximum pressure ratio attained at design speed was 1.53, while maximum weight flow was 38.7 pounds per second per square foot.

At 110 percent design speed a peak efficiency and a maximum pressure ratio of 0.84 and 1.63, respectively, were obtained. Maximum weight flow at 110 percent design speed was 39.3 pounds per second per square foot. Peak efficiencies of 0.98, 0.98, 0.96, and 0.93 were obtained at 60, 70, 80, and 90 percent of design speed, respectively.

Although the given rotor was designed for a tip speed of 1100 feet per second, the performance of the rotor at 90 percent of design speed warrants consideration for the design of an inlet stage. At 90 percent design speed the rotor produced a pressure ratio of 1.38 at a specific weight flow of 37.5 pounds per second per square foot and an efficiency of 0.93. At 80 percent design speed the rotor produced a pressure ratio of 1.29 at a specific weight flow of 36.0 pounds per second per square foot of frontal area at an efficiency of 0.96.

Flow Parameters

Rotor inlet flow parameters. - The rotor inlet flow parameters of inlet axial Mach number, inlet relative Mach number, and inlet relative air angle are presented in figures 3, 4, and 5 for three values of weight flow at 100, 90, and 80 percent of design speed. The three values of weight flow presented for each speed represent the range of weight flows covered and are shown as points A, B, and C (at each speed) on the over-all performance map (fig. 2). Point A represents the near maximum weight flow, point B the near peak efficiency weight flow, and point C the minimum weight flow obtained.

Included in figure 3 are the respective design values of the rotor inlet flow parameters. The distribution of the axial Mach number at design speed agrees with the predicted design values, but the magnitude is low because of the lower than design value of weight flow obtained (fig. 3(a)). It therefore appears that the method employed for obtaining the axial-velocity distribution at the rotor inlet, where the actual radial entropy gradient is negligible, is quite satisfactory. In contrast, it should be noted that the simplified one-dimensional choking analysis of reference 9 which was incorporated into the design system was not satisfactory, in that the design weight flow and axial Mach number could not be attained. The loss in weight flow was probably caused by three-dimensional flow limitations. This three-dimensional choking problem has been successfully handled in turbines with subsonic inlet relative velocities by means of a channel-flow approach (ref. 10). Unfortunately, the supersonic inlet relative Mach numbers together with the range of solidities and inlet flow angles encountered in transonic compressors normally preclude the use of channel-flow techniques. These data do manifest an area for further compressor research, however, particularly for application to compressors whose flow rates approach the theoretical maximum. As shown by figures 3(b) and (c), the lower than design value of inlet Mach number decreased the inlet relative Mach number and increased the inlet relative air angle with reference to their respective design values; however, the radial distribution agrees with the design distribution.

Rotor outlet flow parameters. - The radial variation of the rotor flow parameters dimensionless work coefficient, efficiency, total-pressure ratio, total-pressure-loss coefficient, deviation angle, absolute outlet angle, relative outlet angle, absolute outlet Mach number, relative outlet Mach number, static-pressure-rise coefficient, diffusion factor, and axial-velocity ratio are presented in figures 6, 7, and 8 for design, 90 percent design, and 80 percent design speed at the weight-flow values shown in the over-all performance map (fig. 2). The curves of the outlet flow parameters at design speed (fig. 6) include the respective design parameters for the design weight flow of 40 pounds per second per square foot of frontal area. In comparing the outlet design flow parameters, it should be noted that the design parameters were based on a weight flow of 40 pounds per second per square foot, which was not obtained because of three-dimensional flow limitations. Therefore, the methods of determining such flow parameters as loss coefficient, deviation angle, and flow distribution cannot be adequately evaluated. Furthermore, the three-dimensional effects which apparently exist may limit the applicability of the basic blade-element approach used in this design.

At the low weight flow the energy addition (work coefficient) increased with radius from the rotor hub to the rotor tip (fig. 6(a)). As the weight flow was increased, the energy addition tended to decrease from the mean radius to the tip. At the highest weight flow the energy

addition decreased across the passage from the rotor hub to the rotor tip. At the near peak efficiency weight flow of 38.34 pounds per second per square foot of frontal area, the work coefficient was approximately 10 percent lower at the hub section than the radial constant design value of 0.332 and approximately 5 percent above this value at the tip section (10 percent of the passage height from the outer wall).

At all weight flows the efficiency increased slightly from the rotor hub to the mean radius and decreased sharply from the mean radius to the rotor tip (fig. 6(b)). At the peak efficiency weight flow the efficiency increased from 0.97 at the hub section (90 percent of the passage height from the outer wall) to 0.99 at the mean radius and then decreased sharply to 0.76 at the tip section (10 percent of the passage height from the outer wall). The efficiency over the lower half of the blade at the peak efficiency weight flow was near or above the blade-element design values, which varied from 0.98 at the inner wall to 0.95 at the outer wall.

The total-pressure ratio varied in accordance with the energy addition and efficiency variations (fig. 6(c)). At the lower weight flows the combination of the energy addition and efficiency resulted in the total-pressure ratio increasing from the rotor hub to a peak value at the mean radius and then decreasing from the mean radius to the rotor tip. At the high weight flow the combination of the energy addition and the efficiency resulted in the total-pressure ratio more or less decreasing continually from the rotor hub to the rotor tip. The total-pressure ratio was lower than the design value in the blade end regions and above the design value at the mean radius.

The total-pressure-loss coefficient had a minimum value at the mean radius and in general increased to the blade end regions (fig. 6(d)). At the near peak efficiency weight flow of 38.34 pounds per second per square foot of frontal area the total-pressure-loss coefficient increased from the minimum value of 0.01 at the mean radius to 0.045 at the hub section, and to 0.174 at the tip section.

The deviation angle only approached the design distribution at the high weight flow (fig. 6(e)). At the high weight flow the deviation angle was approximately $3\frac{1}{2}^{\circ}$ high at the hub section, within 1° at the midpoint in the passage, and approximately 2° high at the tip section. At lower weight flows the deviation angles were low over a major portion of the passage. Perhaps the low values of the deviation angle are a result of the three-dimensional flows previously mentioned.

The outlet relative Mach number near the peak efficiency weight flow was higher than the design value at the hub region and lower than the design value at the tip region (fig. 6(f)). The variation can be partly due to the low rotor tip efficiency, which reduced the flow in the tip

region and forced the flow toward the hub section, and partly due to the lower than design weight flow obtained. As stated previously, the design outlet velocity distributions were obtained assuming no change in entropy in the radial direction (constant total-pressure-loss coefficient). Therefore, as is pointed out in reference 11, with the decreased efficiency toward the rotor tip the entropy gradient would cause the velocity to be lower than the design value at the rotor tip and higher than the design value at the rotor hub. The average level of the outlet relative Mach number is high because the increased loss increased the specific outlet flow and therefore increased the outlet relative Mach number.

The combination of outlet relative Mach number, deviation angle, and wheel speed resulted in the absolute outlet angle variation of figure 6(g). At the near peak efficiency weight flow the absolute outlet-air angle was approximately 5° low and 5° high at the hub and tip sections, respectively. The absolute outlet Mach number, which is also a function of the relative outlet Mach number, deviation angle (or relative outlet-air angle), and wheel speed, is presented in figure 6(h). The absolute outlet Mach number at the near peak efficiency weight flow was 1.03 at the hub (0.10 higher than design) and 0.80 at the tip (0.06 lower than design).

The axial-velocity ratio across the rotor (fig. 6(i)) was higher than the design value at all weight flows except at the rotor tip section. At the rotor tip section the axial-velocity ratio dropped below the design value at the lower weight flows. The higher than design values of the axial-velocity distribution can be attributed to high outlet specific weight flow caused by the lower than design value of efficiency.

The blade loading parameters, diffusion factor, and static-pressure-rise coefficient are presented in figures 6(j) and (k). In general, the diffusion factor was lower than the design values near the inner wall and above the design values toward the outer wall, while the static-pressure coefficient was in general lower than design conditions at all radii. This variation in the blade loading parameter was primarily due to the resultant axial-velocity distribution after the rotor.

The rotor flow parameters for 90 and 80 percent of design speed are presented in figures 7 and 8. These data are presented to give more detailed information on the rotor performance, since the 90 and 80 percent design speeds are still in the realm of transonic rotor design conditions. These conditions also represent good potential inlet stage designs.

Blade-element flow parameters. - The blade-element flow parameters (total-pressure-loss coefficient, relative inlet Mach number, axial-velocity ratio, static-pressure-rise coefficient, efficiency, deviation angle, diffusion factor, and dimensionless work coefficient) are

presented in figure 9 as functions of the incidence angle for the five major radial stations at 70, 90, 100, and 110 percent design speed. The extensive blade-element data are presented to further supplement the published data on transonic rotor blade performance. In addition, the blade-element flow parameters at optimum incidence angle obtained from these curves are used in the discussion that follows.

RADIAL MATCHING OF BLADE-ELEMENT SECTIONS

The radial matching of the blade-element incidence angles is presented in figure 10 at design speed. Incidence angle is plotted against radius for various weight flows at design speed (shown as data points). Included in figure 10 are the minimum-loss incidence angles obtained from the blade-element data of figure 9 (solid curve) and the design minimum-loss incidence angles (dashed curve, ref. 8) for each of the five blade-element sections. As shown by figure 10, the radial incidence-angle variation at a weight flow of 38.34 pounds per second per square foot was 2° to 3.1° higher than the design values of minimum-loss incidence angle across the blade passage. Although the incidence-angle variation at the weight flow of 38.34 pounds per second per square foot was higher than the design values of the minimum-loss incidence angles, the incidence-angle variation was within 1° of the measured minimum-loss incidence angle at all radii. For this reason a good over-all peak efficiency of 0.89 was obtained (fig. 2), but at a weight flow 4.1 percent lower than the design value.

COMPARISON OF BLADE-ELEMENT PARAMETERS WITH DESIGN RULES

A comparison of the measured blade-element parameters with those computed from the equations of reference 8 is presented in table II of the report. The measured blade-element performance parameters (incidence angle, deviation angle, and relative total-pressure-loss coefficient) were obtained from figure 9 for each blade-element section at the minimum-loss incidence angle. The computed values are not the design values but rather computations based on the measured relative inlet Mach number, relative inlet-air angle at minimum-loss incidence angle, and required blade geometry. This method of comparison was chosen because the design inlet conditions were not realized. The calculated values of minimum-loss incidence angle, deviation angle, and relative total-pressure-loss coefficient are tabulated in table II for the five major radial positions at design speed.

As shown by table II, the minimum-loss incidence angle was 0.9° to 4.1° greater than the values predicted by the design rule. The deviation angle at the minimum-loss incidence angle was 0.4° to 4.6° less than

4713

CA-2 back

predicted design-rule values from the outer wall to section D (30 percent from the inner wall); however, the inner-wall section deviation angle was 3.5° greater than the predicted design-rule values. The total-pressure-loss coefficient is presented in table II as $\bar{w} \cos \beta_2 / 2\sigma$ in order to be consistent with the design-rule data of reference 8. The total-pressure-loss parameter is approximately three times greater than the predicted design-rule value at the outer-wall sections (10 and 30 percent) and approximately double the design-rule value at the inner-wall section; however, the 50-percent and 70-percent sections show very close agreement with the design-rule values.

Since the losses encountered across blade elements with transonic inlet Mach numbers are affected by the occurrence of passage shock, the shock losses were approximated using the simplified two-dimensional flow model described in reference 12. The shock losses thus obtained are presented together with the total losses in figure 11 as a function of inlet relative Mach number. The data of figure 11 pertain only to the near optimum incidence angle and show that the tip loss increases with inlet relative Mach number. The low indicated values of the profile loss (difference between the total and shock losses) can be attributed to the tapered rotor tip, as pointed out in reference 12. By contouring the rotor tip, some three-dimensional compression (reduction of streamline spacing) of the supersonic flow can be obtained, and it results in a lower local Mach number than that obtained in the simplified two-dimensional solution. Apparently the calculated shock losses are overestimated because of the three-dimensional effects in the supersonic flow. The results indicate, however, that the high losses in the tip region are primarily due to high Mach numbers and shock losses and not to blade loading. For example, the computed suction-surface Mach number at the tip section for design speed was 1.90, and the diffusion factor was approximately 0.25.

Although the agreement between the test data and the design-rule predictions is not considered good, the minimum-loss incidence angles were matched radially (fig. 10) so that good compressor efficiency was obtained at a weight flow about 4 percent below the design value.

SUMMARY OF RESULTS

The major results obtained from the investigation of the 0.35 hub-tip radius ratio, axial-flow, inlet-stage rotor are as follows:

1. At the design equivalent tip speed of 1100 feet per second, a total-pressure ratio of 1.51 was obtained at an equivalent specific weight flow of 38.0 pounds per second per square foot of frontal area, and the adiabatic-temperature-rise efficiency was 0.89. Peak efficiencies of 0.98, 0.98, 0.96, 0.93, and 0.84 were obtained at 60, 70, 80, 90, and 110 percent of design speed, respectively.

2. The performance at 80 and 90 percent design speed also makes this rotor appear highly suitable for use as a transonic inlet stage on present engines. At 90 percent design speed the rotor produced a pressure ratio of 1.38 at a specific weight flow of 37.5 pounds per second per square foot of frontal area and an adiabatic efficiency of 0.93. At 80 percent design speed the rotor produced a pressure ratio of 1.29 at a specific weight flow of 36.0 pounds per second per square foot of frontal area and an efficiency of 0.96.

3. The design weight flow was not obtained primarily because of three-dimensional flow limitations.

4. A method of calculating the axial-velocity distribution before and after a rotor is presented. At the rotor inlet the calculated velocity distribution was good. At the rotor outlet the calculated axial-velocity distribution was poor primarily because the assumed flow conditions were not obtained.

5. Because of good radial selection of the blade-element parameters, good compressor efficiency was obtained, but at a weight flow below the design value.

6. The underestimation of the rotor losses resulted in higher than design outlet velocities.

7. The high loss at the rotor tip section appears to be primarily a function of shock losses caused by high suction-surface Mach numbers.

Lewis Flight Propulsion Laboratory
National Advisory Committee for Aeronautics
Cleveland, Ohio, June 19, 1958

APPENDIX A

SYMBOLS

A_F	compressor frontal area, sq ft
c	blade chord, in.
c_p	specific heat at constant pressure, Btu/(lb)(°R)
c_v	specific heat at constant volume, Btu/(lb)(°R)
D	diffusion factor
g	acceleration due to gravity, 32.17 ft/sec ²
H	total enthalpy, ft-lb/lb
i	angle of incidence, angle between tangent mean camber line at leading edge and inlet-air direction, deg
J	mechanical equivalent of heat, 778.2 ft-lb/Btu
K	constant
M	Mach number
P	total pressure, lb/sq ft
p	static pressure, lb/sq ft
r	radius, in.
T	total temperature, °R
t	blade thickness, in.
U	blade speed, ft/sec
V	velocity of air, ft/sec
w	integrated weight flow at rotor inlet, lb/sec
β	air angle, angle between air velocity vector and axial direction, deg
γ	ratio of specific heats, c_p/c_v

- 4713
- δ ratio of inlet total pressure to NACA standard sea-level pressure of 2116.2 lb/sq ft
- δ° deviation angle, angle between outlet-air direction and tangent to mean camber line at trailing edge, deg
- η adiabatic efficiency
- θ ratio of inlet total temperature to NACA standard sea-level temperature of 518.7° R
- ρ flow density, lb/cu ft
- σ solidity, ratio of blade chord to blade spacing
- φ blade camber angle, difference between angles of tangents to mean camber line at leading and trailing edges, deg
- $\bar{\omega}$ total-pressure-loss coefficient

Subscripts:

- d design rule
- h hub
- id ideal
- min minimum loss
- s shock
- sl NACA standard sea-level conditions
- t tip
- z axial direction
- θ tangential component
- 1 rotor inlet
- 2 rotor outlet

Superscript:

- ' relative

APPENDIX B

EQUATIONS

The equations used for the blade-element and over-all performance are given in this appendix.

Over-All Performance

- (1) Mass-averaged adiabatic-temperature-rise efficiency

$$\eta = \frac{\int_{r_{h,2}}^{r_{t,2}} \rho_2 V_{z,2} r_2 \left[\left(\frac{P_2}{P_1} \right)^{\frac{\gamma-1}{\gamma}} - 1 \right] dr_2}{\int_{r_{h,2}}^{r_{t,2}} \rho_2 V_{z,2} r_2 (T_2 - T_1) dr_2}$$

- (2) Mass-averaged total-pressure ratio

$$\frac{P_2}{P_1} = \left\{ \frac{\int_{r_{h,2}}^{r_{t,2}} \rho_2 V_{z,2} r_2 \left[\left(\frac{P_2}{P_1} \right)^{\frac{\gamma-1}{\gamma}} - 1 \right] dr_2}{\int_{r_{h,2}}^{r_{t,2}} \rho_2 V_{z,2} r_2 dr_2} + 1.0 \right\}^{\frac{\gamma}{\gamma-1}}$$

Rotor Blade Element

- (1) Blade-element adiabatic-temperature-rise efficiency

$$\eta = \frac{\left(\frac{P_2}{P_1} \right)^{\frac{\gamma-1}{\gamma}} - 1}{\frac{T_2}{T_1} - 1}$$

(2) Relative total-pressure-loss coefficient

$$\bar{\omega} = \left(\frac{P_2}{P_1}\right)_{id} \left[\frac{1 - \left(\frac{P_2}{P_1}\right) \left(\frac{T_1}{T_2}\right)^{\frac{\gamma}{\gamma-1}}}{1 - \left(1 + \frac{\gamma-1}{2} M_1'^2\right)^{-\frac{\gamma}{\gamma-1}}} \right]$$

where

$$\left(\frac{P_2}{P_1}\right)_{id} = \left\{ 1 + \frac{\gamma-1}{2} M_R'^2 \left[1 - \left(\frac{r_1}{r_2}\right)^2 \right] \right\}^{\frac{\gamma}{\gamma-1}} = 1$$

for a given rotor design and M_R is the wheel rotational Mach number (outlet wheel tangential velocity divided by inlet relative stagnation velocity of sound).

(3) Dimensionless work coefficient

$$\frac{\Delta H}{U_t^2} = \frac{J g c_p T_{s1} \left(\frac{T_2}{T_1} - 1 \right)}{\left(\frac{U_t}{\sqrt{\theta}} \right)^2}$$

(4) Diffusion factor

$$D = \left(1 - \frac{V_2'}{V_1'} \right) + \frac{V_{\theta 1}' - V_{\theta 2}'}{2\sigma V_1'}$$

REFERENCES

1. Robbins, William H., and Glaser, Frederick, W.: Investigation of an Axial-Flow-Compressor Rotor with Circular-Arc Blades Operating up to a Rotor-Inlet Relative Mach Number of 1.22. NACA RM E53D24, 1953.

2. Serovy, George K., Robbins, William H., and Glaser, Frederick, W.: Experimental Investigation of a 0.4 Hub-Tip Diameter Ratio Axial-Flow Compressor Inlet Stage at Transonic Inlet Relative Mach Numbers. I - Rotor Design and Over-All Performance at Tip Speeds from 60 to 100 Percent of Design. NACA RM E53ILL, 1953.
3. Boxer, Emanuel, and Bernot, Peter T.: Experimental Investigation of a Transonic Axial-Flow-Compressor Rotor Designed for Sonic Inlet Velocity with an Inlet Hub-Tip Radius Ratio of 0.35. NACA RM L56F14, 1956.
4. Westphal, Willard R., and Maynard, John W., Jr.: Design and Investigation of a Transonic Axial-Flow Compressor Rotor with an Inlet Hub-Tip Radius Ratio of Essentially Zero. NACA RM L57A10, 1957.
5. Montgomery, John C., and Glaser, Frederick W.: Experimental Investigation of 0.4 Hub-Tip Diameter Ratio Axial-Flow Compressor Inlet Stage at Transonic Inlet Relative Mach Numbers. III - Effect of Tip Taper on Over-All and Blade-Element Performance. NACA RM E55L09, 1956.
6. Montgomery, John C., and Glaser, Frederick: Experimental Investigation of a 0.4 Hub-Tip Diameter Ratio Axial-Flow Compressor Inlet Stage at Transonic Inlet Relative Mach Numbers. IV - Performance of Tapered-Tip Rotor Configuration with Reset Blade Angles. NACA RM E56L06, 1957.
7. Hatch, James E., and Bernatowicz, Daniel T.: Aerodynamic Design and Over-All Performance of First Spool of a 24-Inch Two-Spool Transonic Compressor. NACA RM E56L07a, 1957.
8. Robbins, William H., Jackson, Robert J., and Lieblein, Seymour: Blade-Element Flow in Annular Cascades. Ch. VII of Aerodynamic Design of Axial-Flow Compressors, vol. II. NACA RM E56B03a, 1956.
9. Wright, Linwood C., and Schwind, Richard: Throat-Area Determination for a Cascade of Double-Circular-Arc Blades. NACA RM E55H25a, 1955.
10. Stewart, Warner L.: Analytical Investigation of Flow Through High-Speed Mixed-Flow Turbine. NACA RM E51H06, 1951.
11. Hatch, James E., Giamati, Charles C., and Jackson, Robert L.: Application of Radial-Equilibrium Condition to Axial-Flow Turbomachine Design Including Consideration of Change of Entropy with Radius Downstream of Blade Row. NACA RM E54A20, 1954.
12. Schwenk, Francis C., Lewis, George W., and Hartmann, Melvin J.: A Preliminary Analysis of the Magnitude of Shock Losses in Transonic Compressors. NACA RM E57A30, 1957.

TABLE I. - ROTOR BLADE DESIGN VALUES AND GEOMETRY

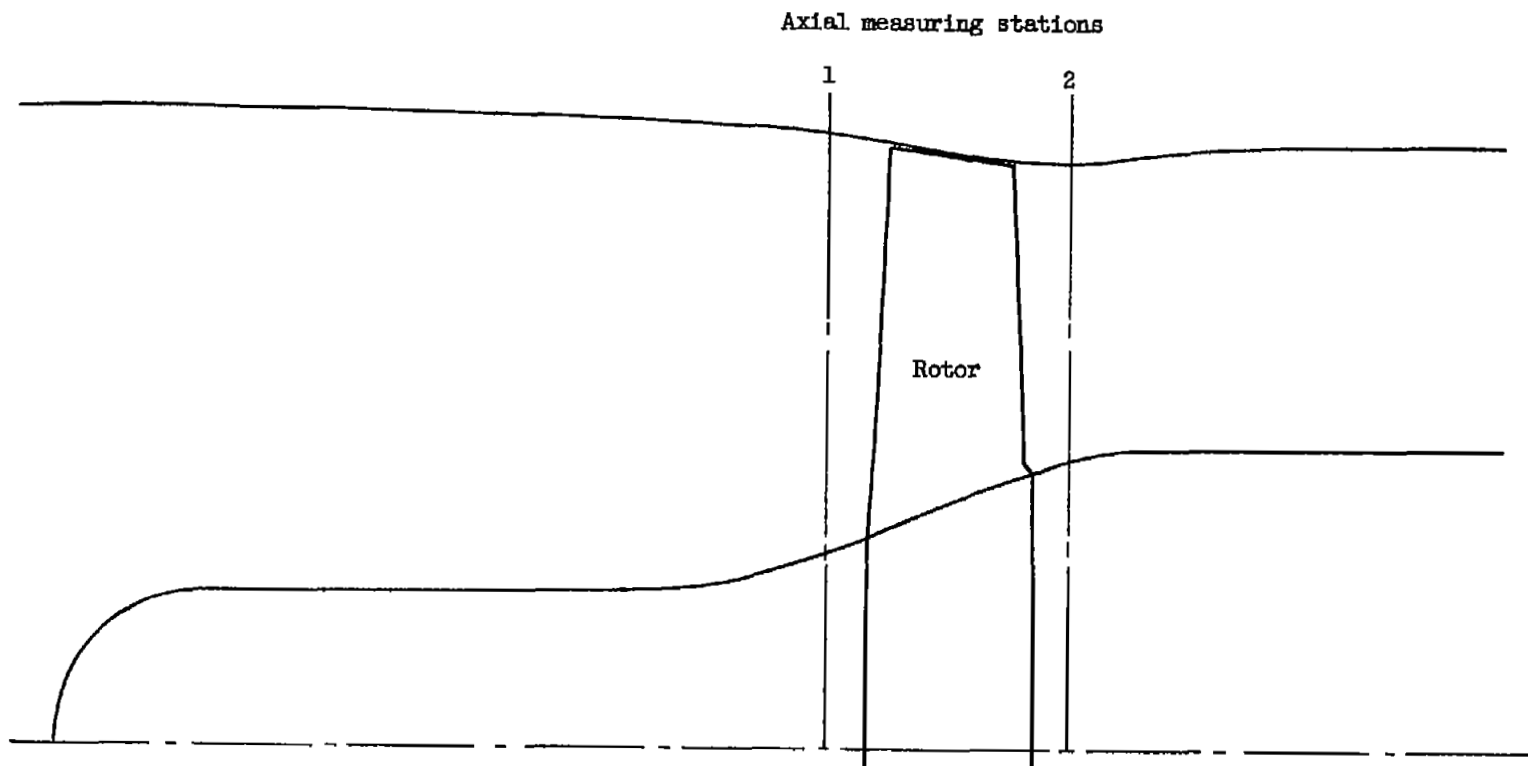
[Ref. 8.]

Passage height from outer wall, percent	Inlet radius, r_1 , in.	Outlet radius, r_2 , in.	Relative inlet-air angle, β_1' , deg	Relative outlet-air angle, β_2' , deg	Blade thickness ratio, t/c	Solidity, σ	Diffusion factor, D	Blade camber angle, ϕ , deg	Relative inlet Mach number, M_1'	Absolute outlet Mach number, M_2	Inclidence angle, i , deg	Deviation angle, δ° , deg
10	6.59	6.44	52.3	35.5	0.053	0.980	0.347	18.2	1.228	0.858	2.8	4.2
30	5.67	5.75	46.9	29.3	.059	1.118	.385	16.1	1.151	.838	5.6	4.0
50	4.75	5.06	41.8	20.2	.065	1.303	.411	19.0	1.059	.840	7.3	4.6
70	3.83	4.37	37.0	7.3	.071	1.558	.397	27.4	.941	.866	8.4	6.1
90	2.91	3.68	31.9	-9.4	.077	1.938	.303	39.7	.809	.930	9.1	7.5

TABLE II. - COMPARISON OF BLADE-ELEMENT PERFORMANCE WITH DESIGN-RULE VALUES

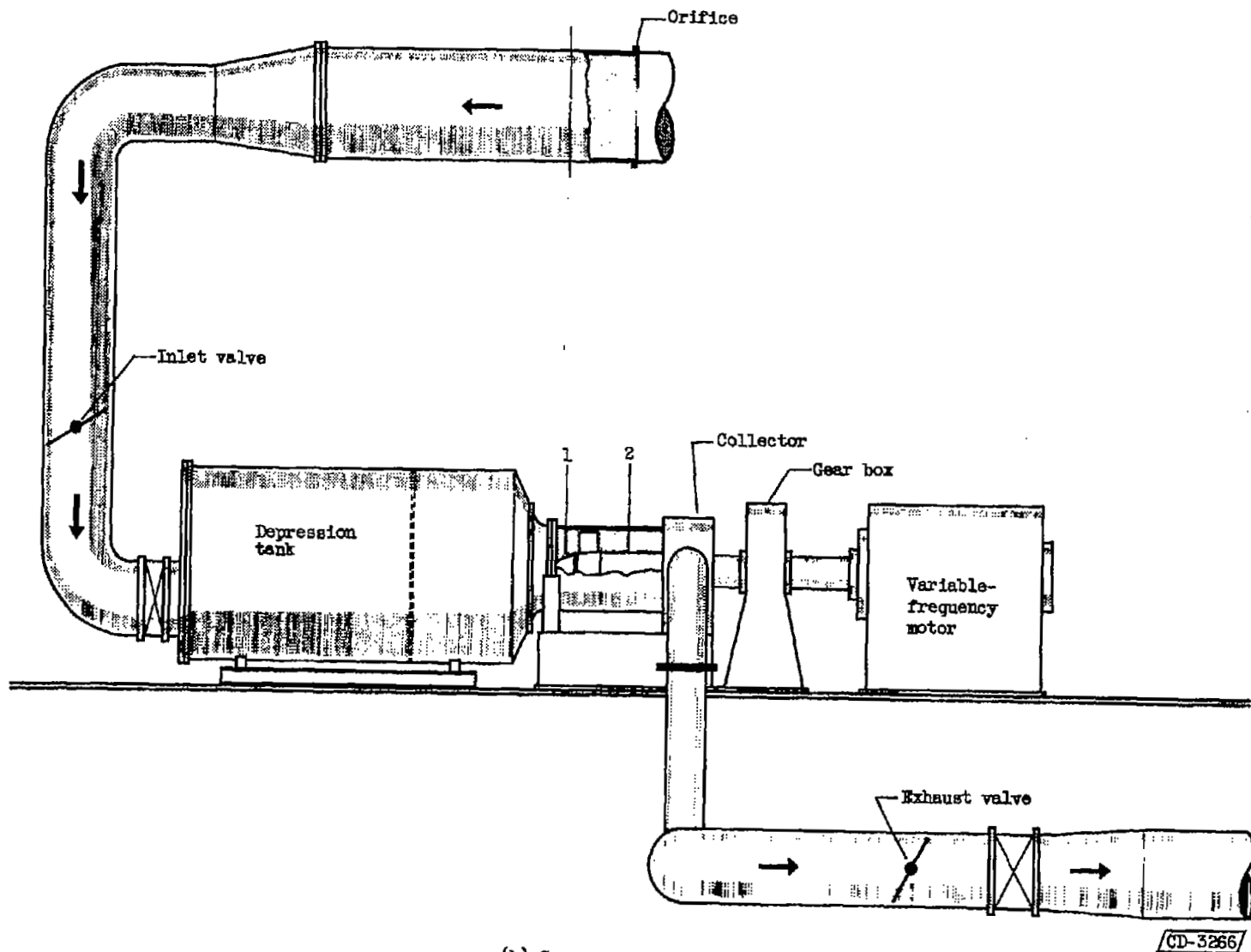
[Design-rule values from ref. 8.]

Passage height from outer wall, percent	Blade camber angle, ϕ , deg	Blade thickness ratio, t/c	Solidity, σ	Relative inlet Mach number, M_1^i	Relative inlet-air angle, β_1^i	Incidence angle, deg			Deviation angle, deg			Total-pressure-loss coefficient	
						Experimental, i_{min}	Design rule, i_d	$i_{min} - i_d$	Experimental, δ^o	Design rule, δ_d^o	$\delta^o - \delta_d^o$	$\frac{\bar{w} \cos \beta_2^i}{2\sigma}$	$\left(\frac{\bar{w} \cos \beta_2^i}{2\sigma}\right)_d$
10	18.2	0.053	0.981	1.205	53.8	4.2	3.3	0.9	4.5	4.9	-0.4	0.043	0.016
30	16.1	.059	1.118	1.103	49.4	8.0	5.7	2.3	4.2	4.6	-.4	.026	.007
50	19.0	.065	1.303	.997	44.7	10.1	7.2	2.9	.5	5.1	-4.6	.010	.008
70	27.4	.071	1.558	.876	40.0	11.4	7.9	3.5	5.8	6.3	-.5	.008	.008
90	39.7	.077	1.938	.740	35.0	12.2	8.1	4.1	11.3	7.8	3.5	.012	.005



(a) Compressor annulus.

Figure 1. - Schematic diagrams of compressor and installation.



(b) Compressor installation.

Figure 1. - Concluded. Schematic diagrams of compressor and installation.

4713

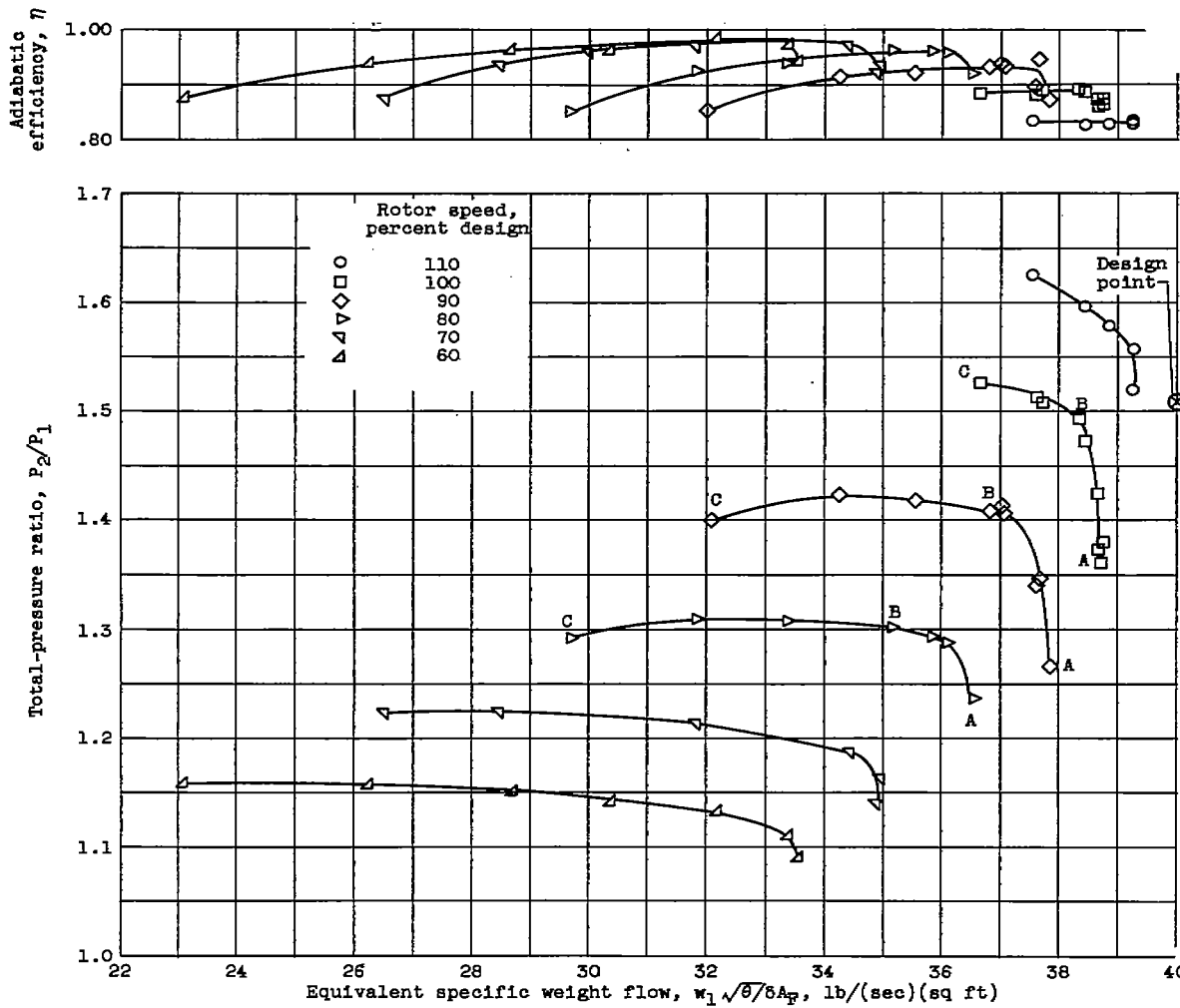


Figure 2. - Mass-averaged over-all performance of rotor with hub-tip diameter ratio of 0.35.

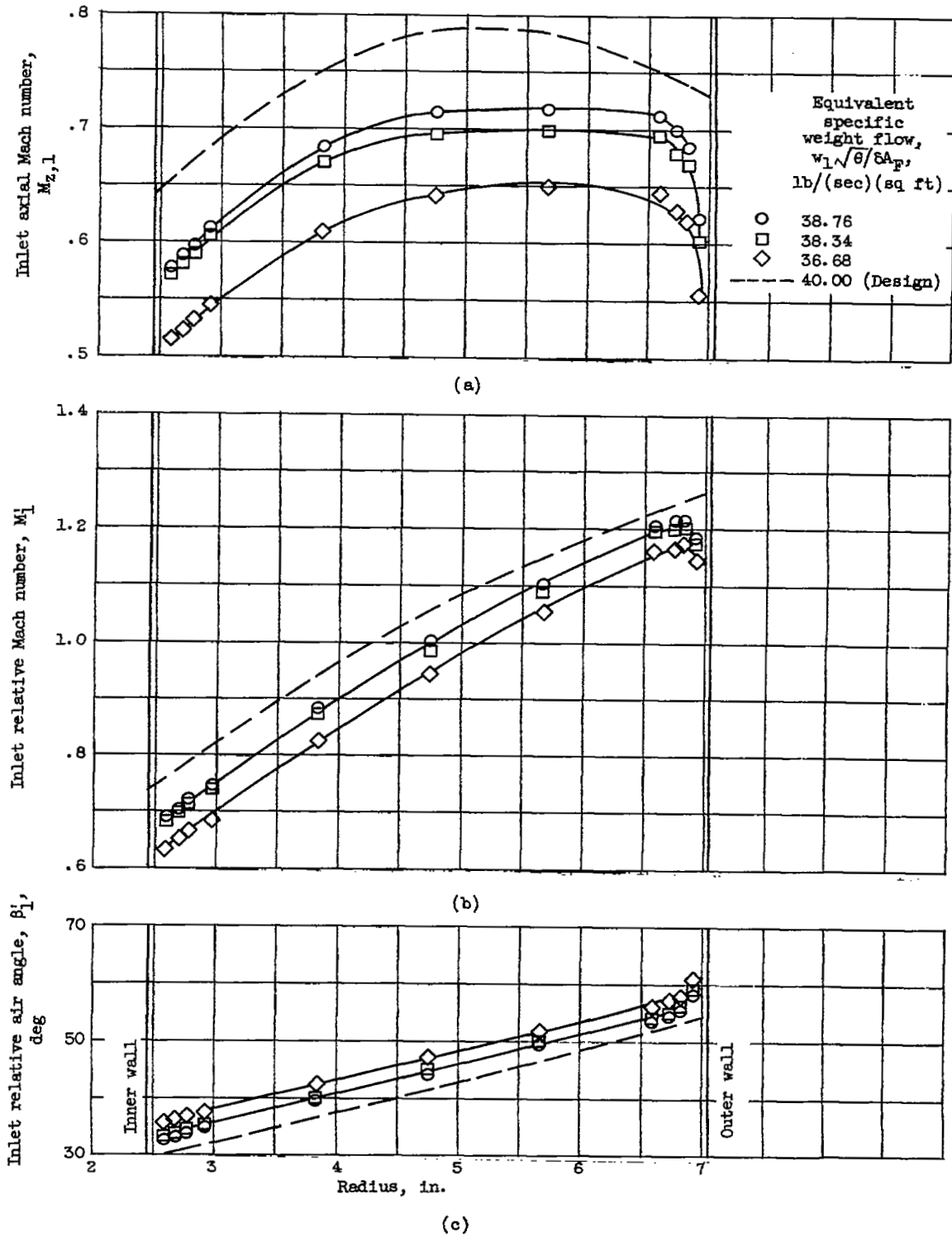


Figure 3. - Radial variation of inlet flow parameters at design speed.

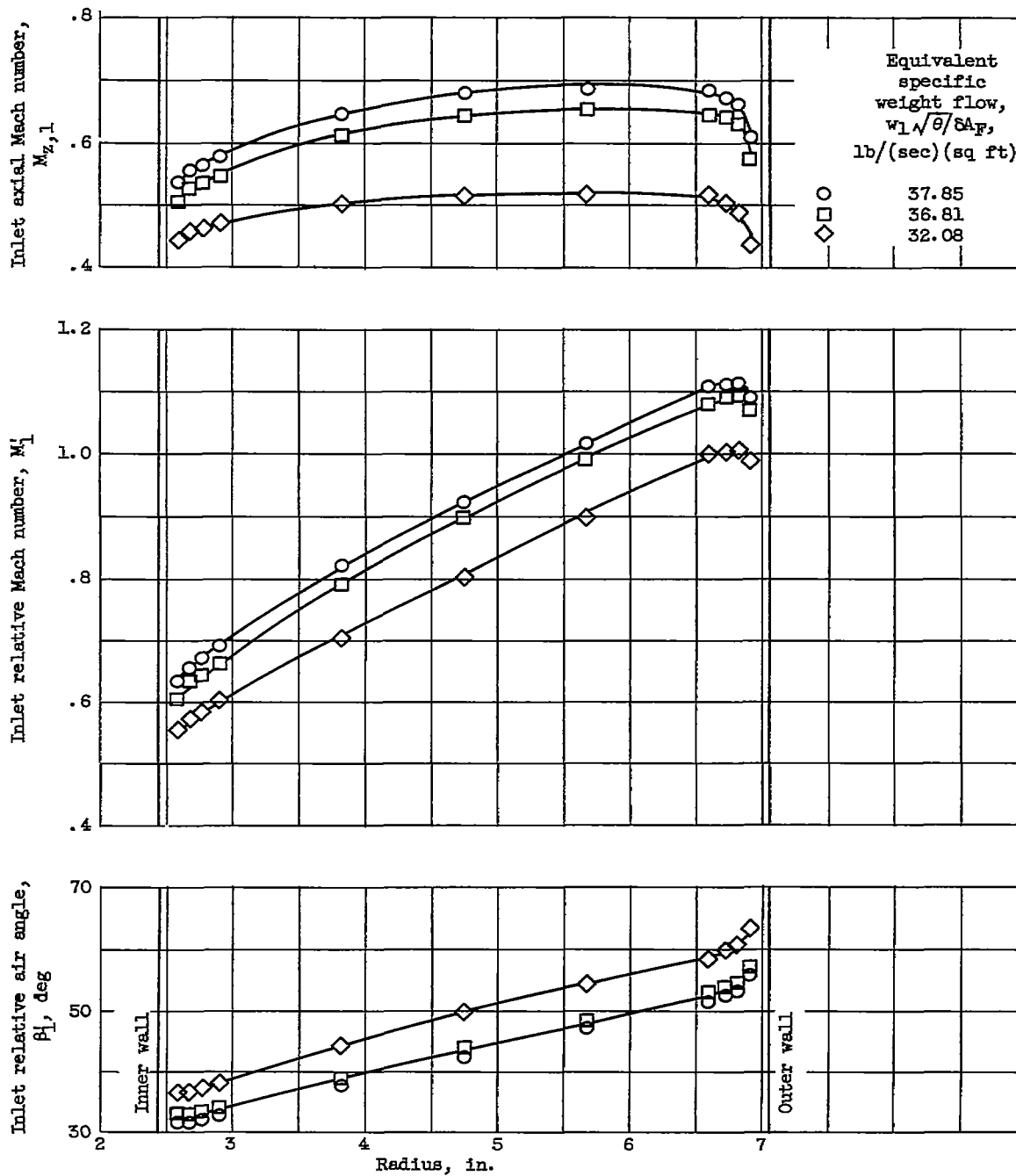


Figure 4. - Radial variation of inlet flow parameters at 90 percent design speed.

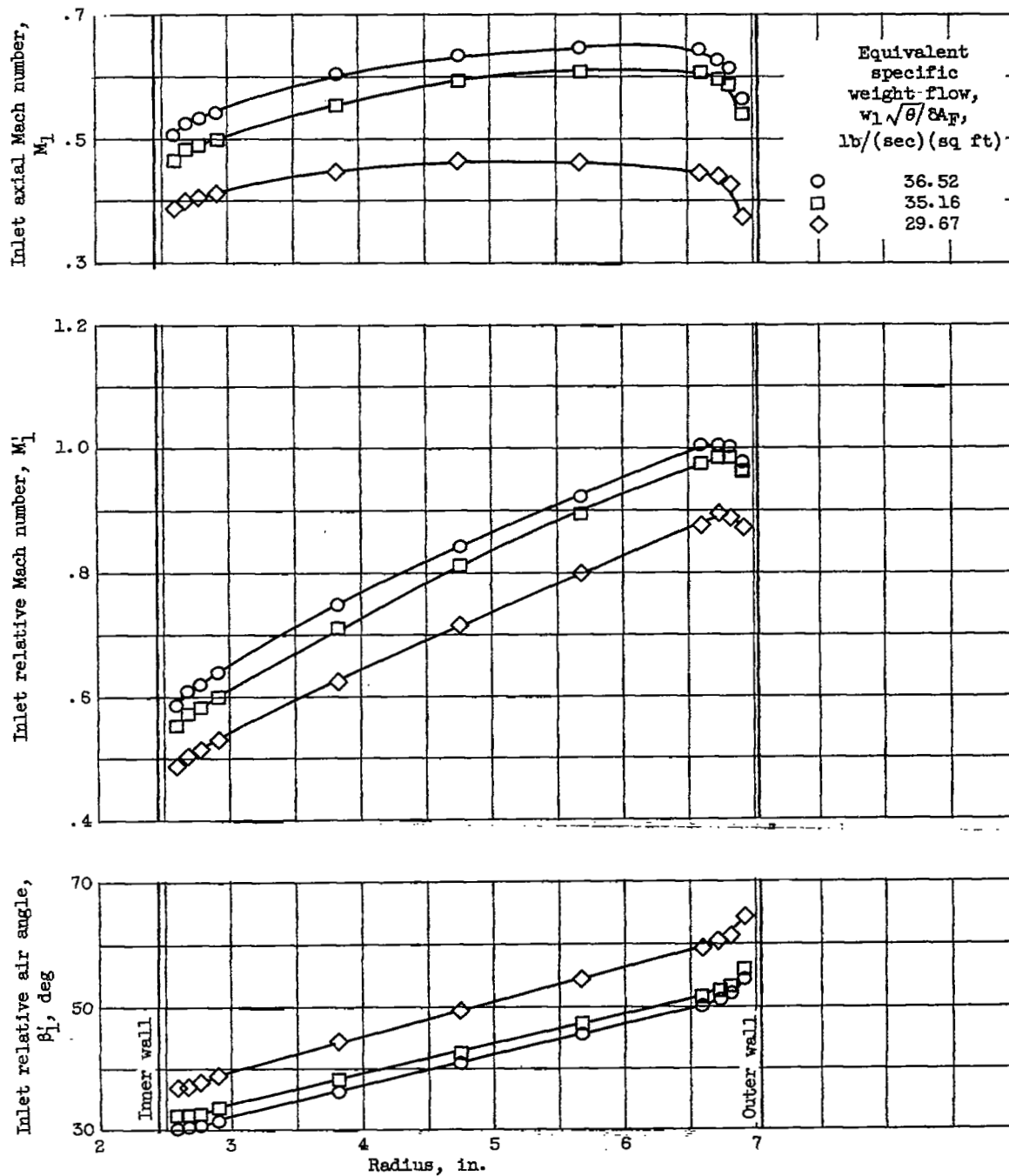


Figure 5. - Radial variation of inlet flow parameters at 80 percent design speed.

4713

CA-4 back

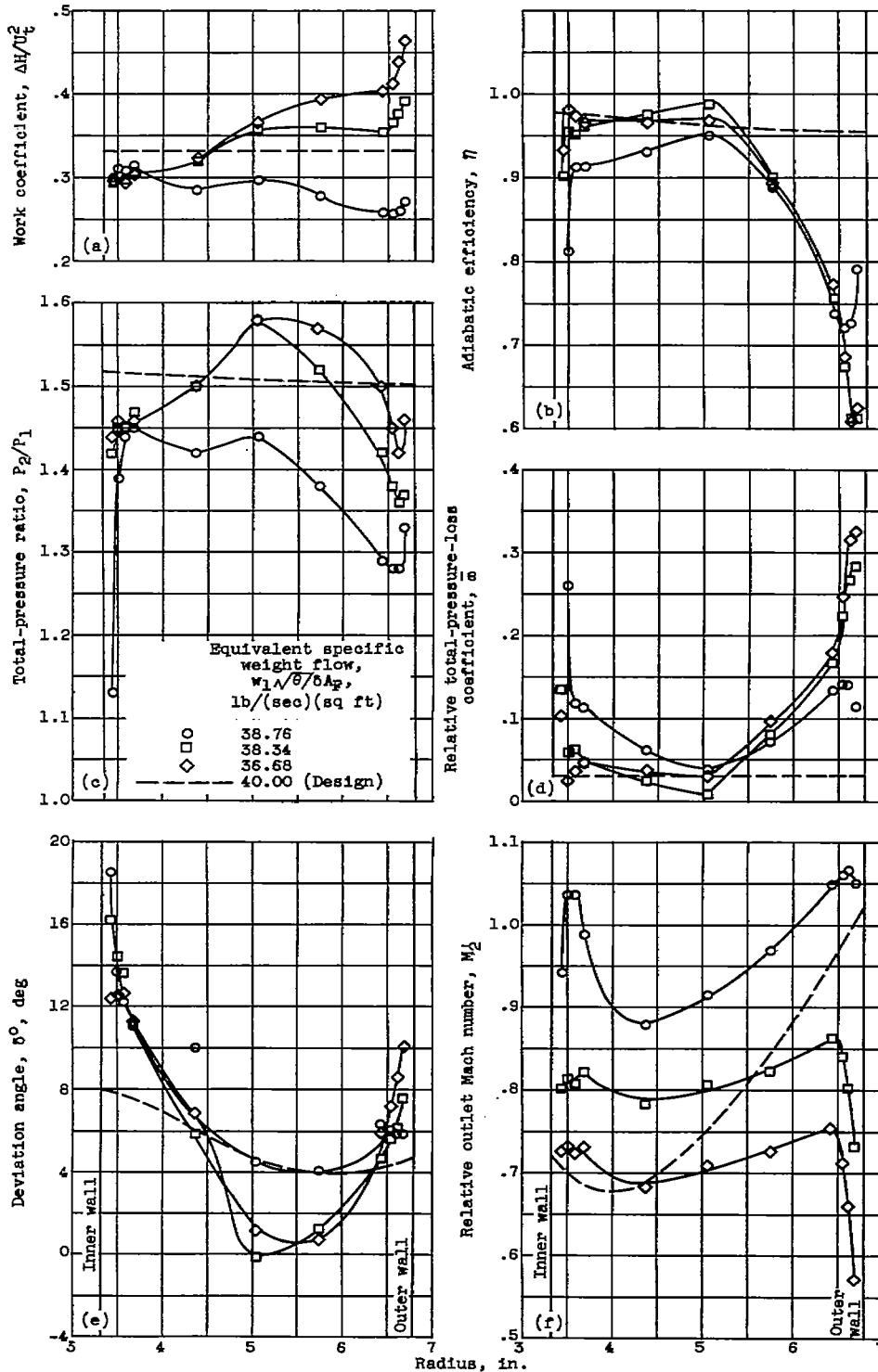


Figure 6. - Radial variation of blade-element and rotor outlet performance at design speed.

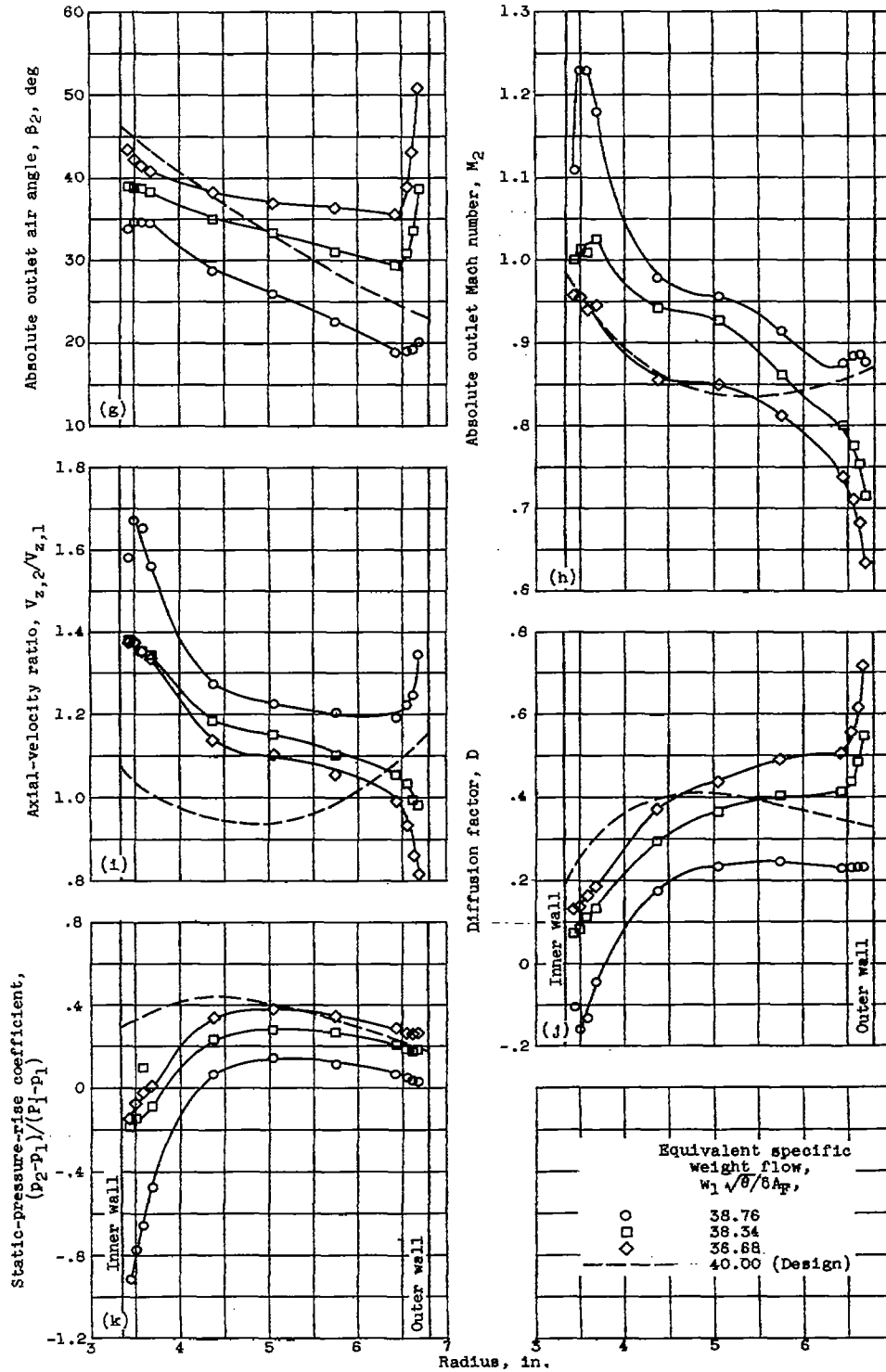


Figure 6. - Concluded. Radial variation of blade-element and rotor outlet performance at design speed.

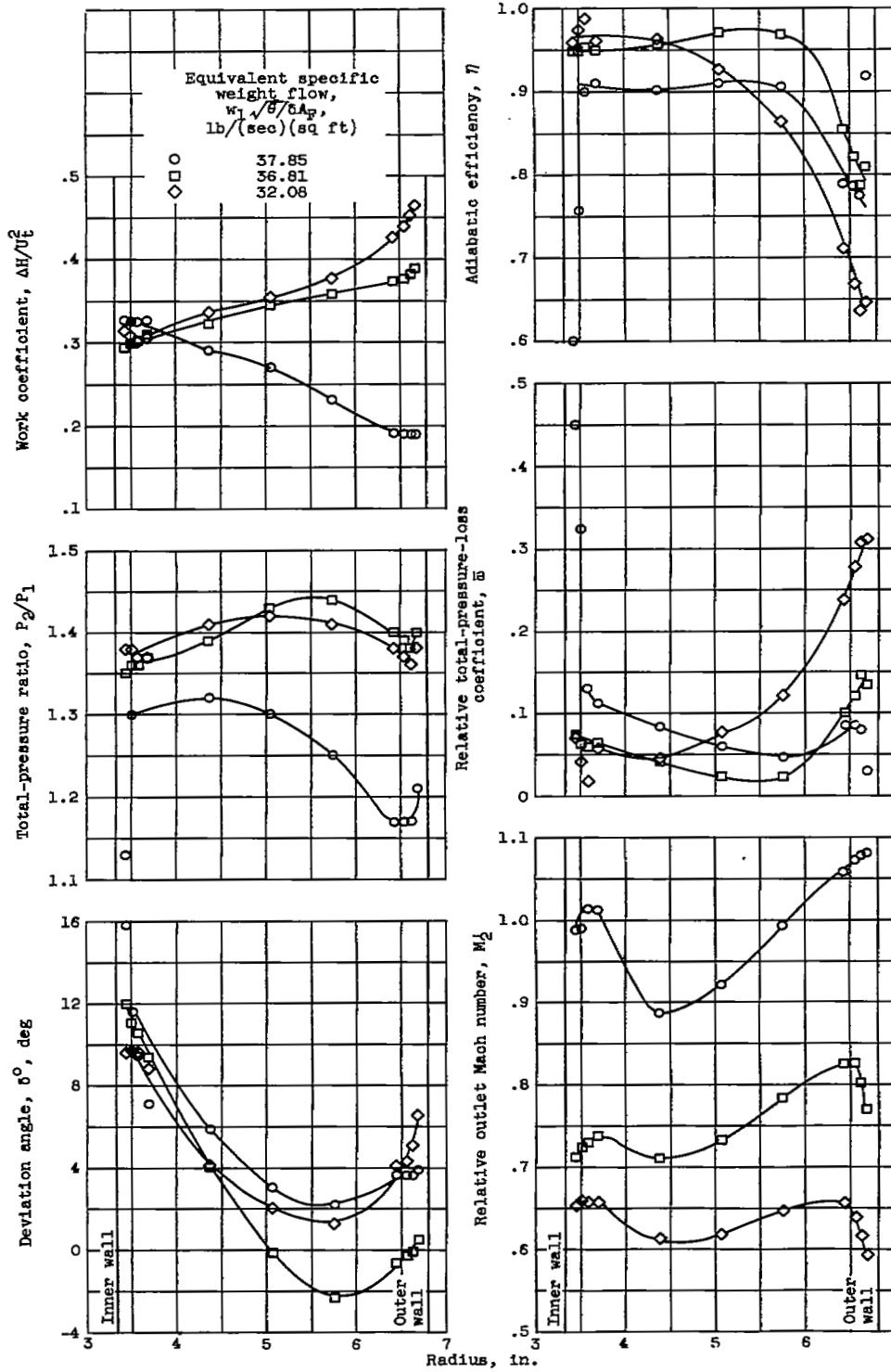
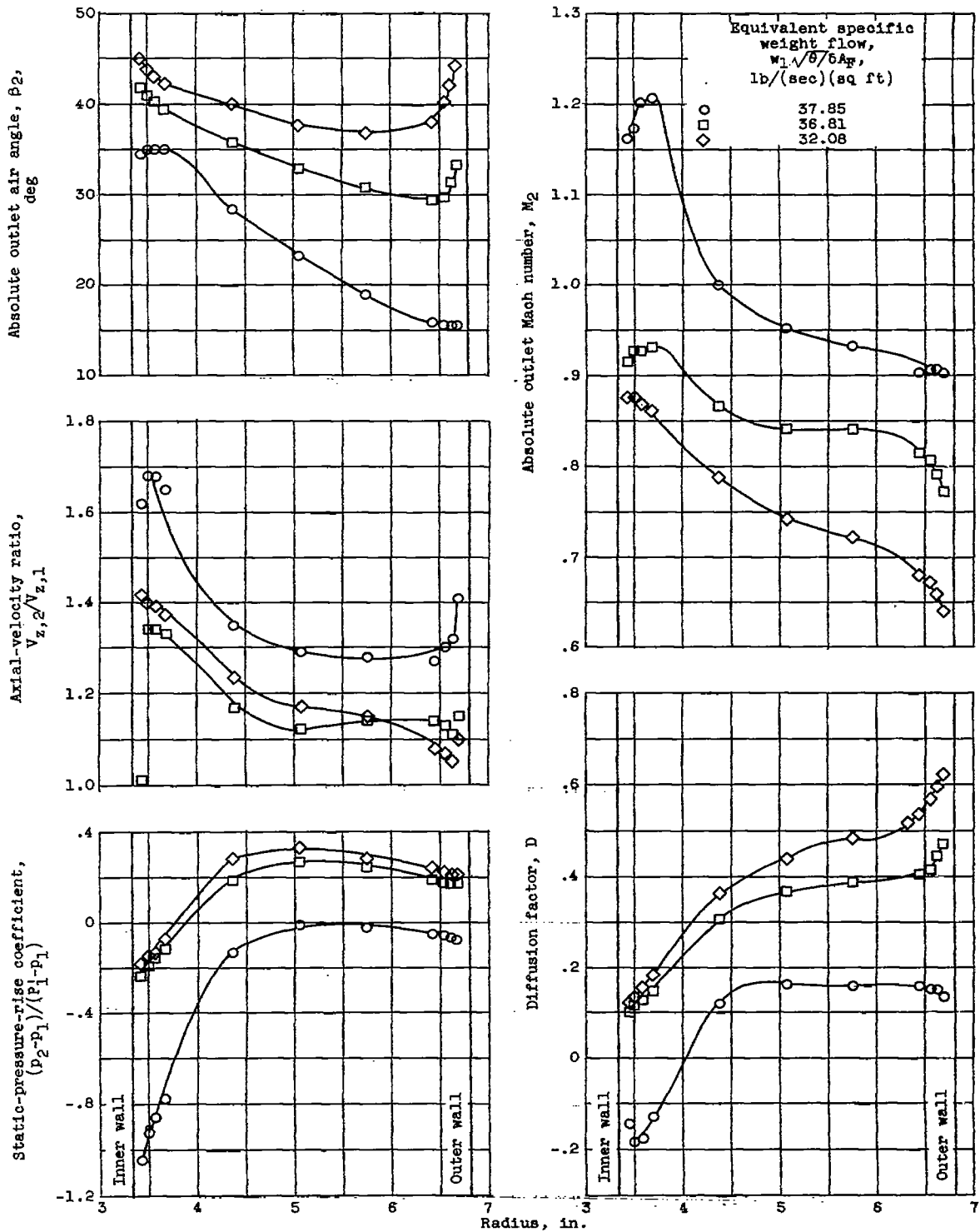


Figure 7. - Radial variation of blade-element and rotor outlet performance at 90 percent design speed.



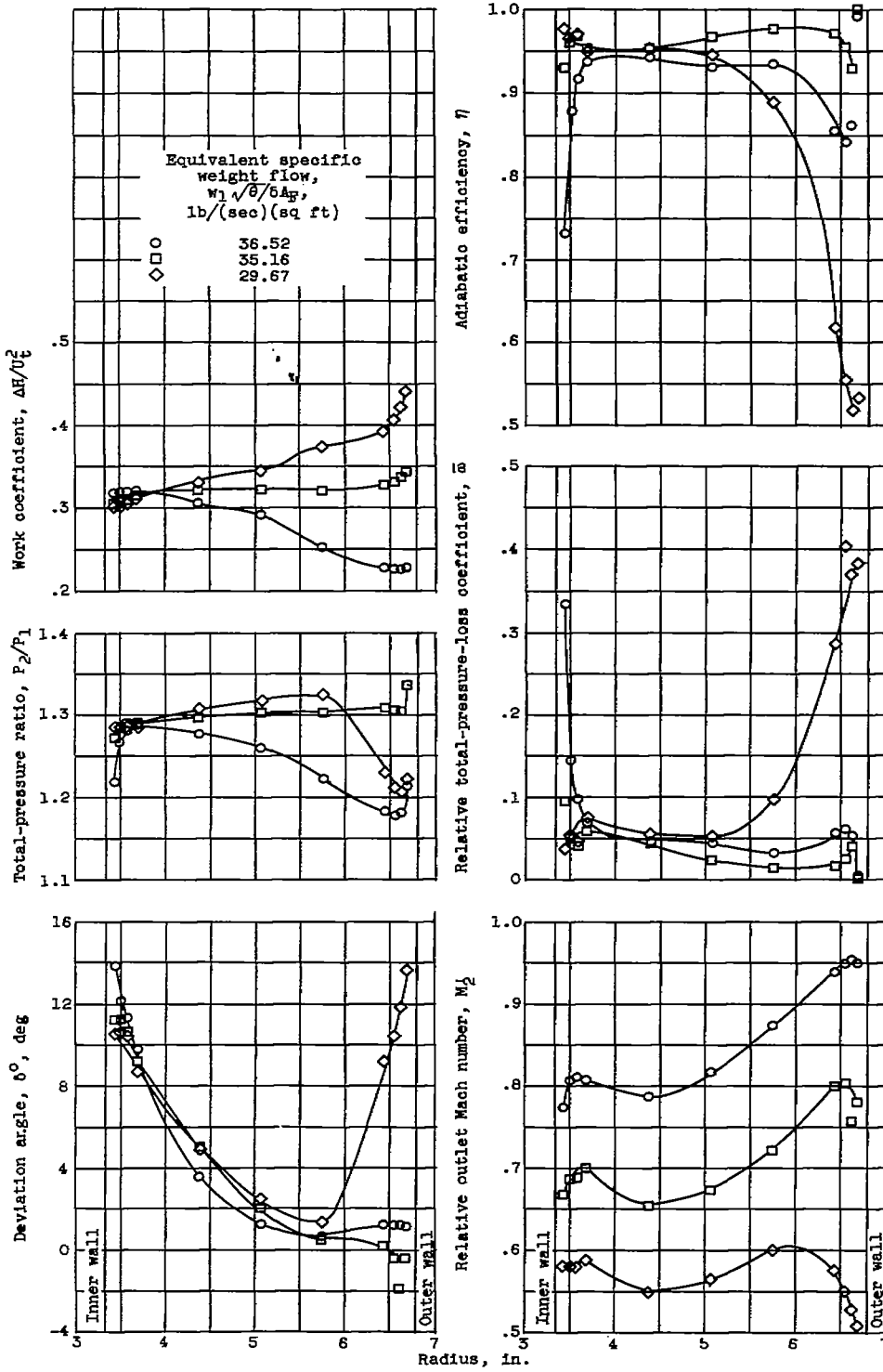


Figure 8. - Radial variation of blade-element and rotor outlet performance at 80 percent design speed.

4713

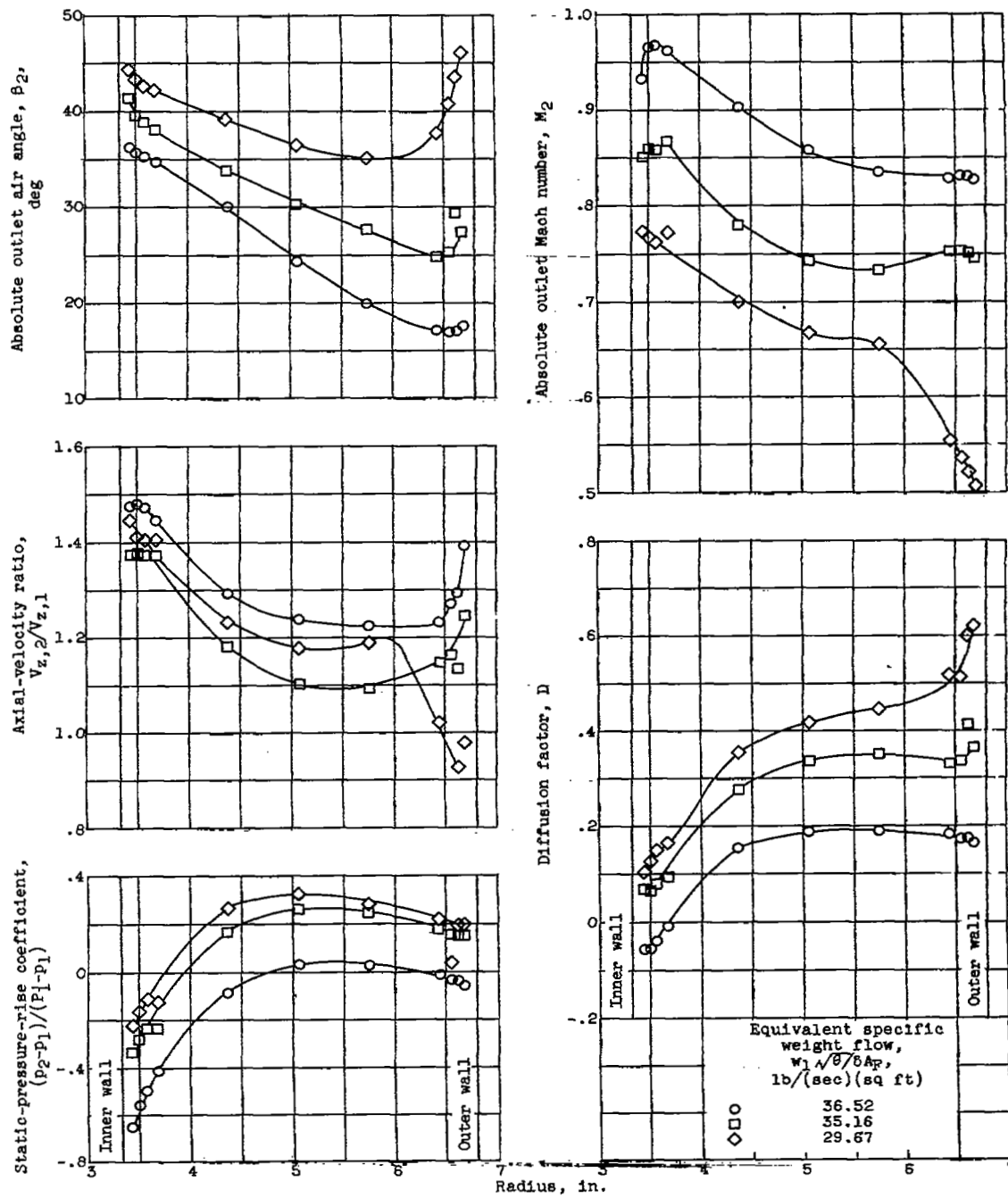
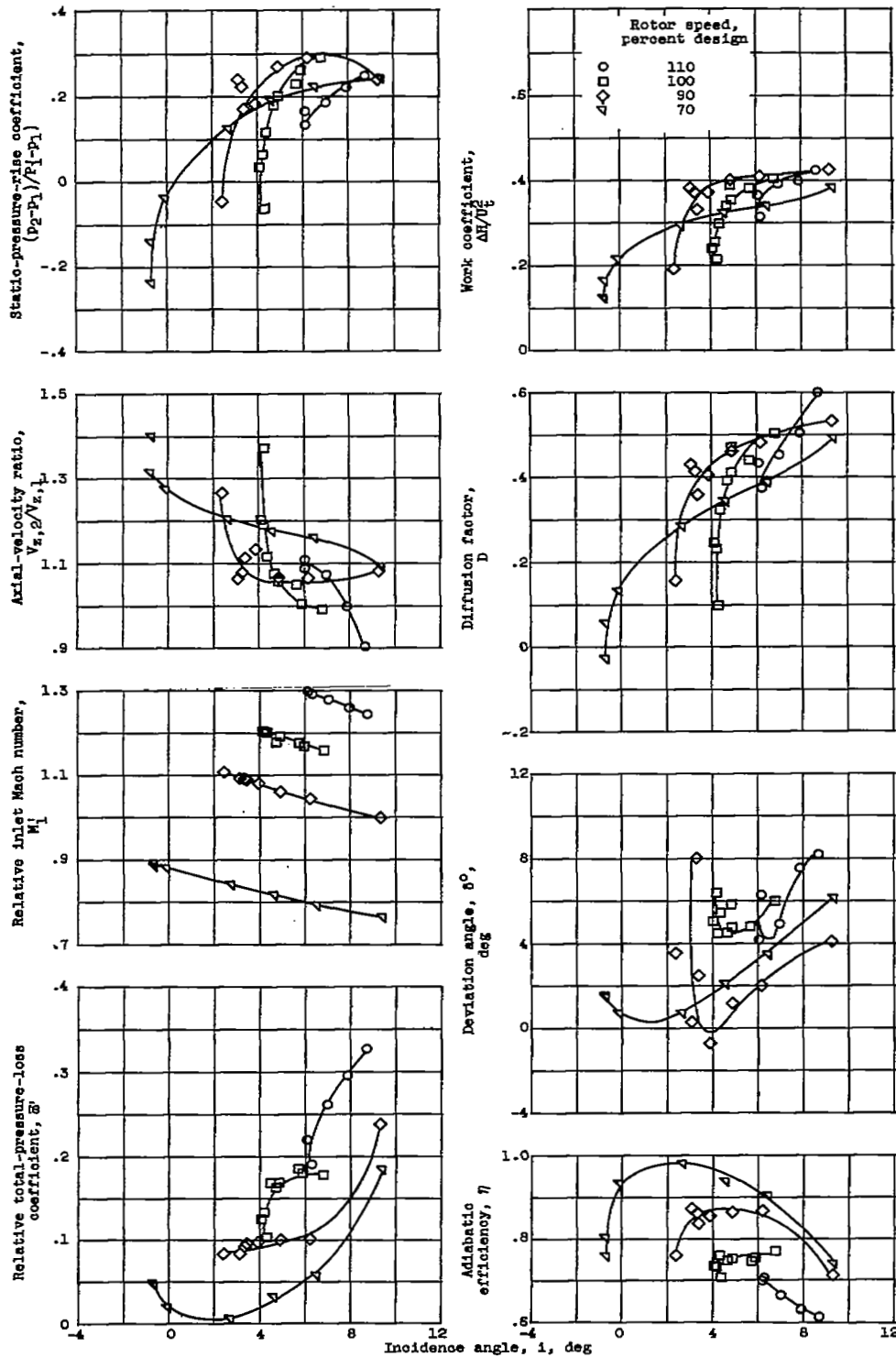


Figure 8. - Concluded. Radial variation of blade-element and rotor outlet performance at 80 percent design speed.

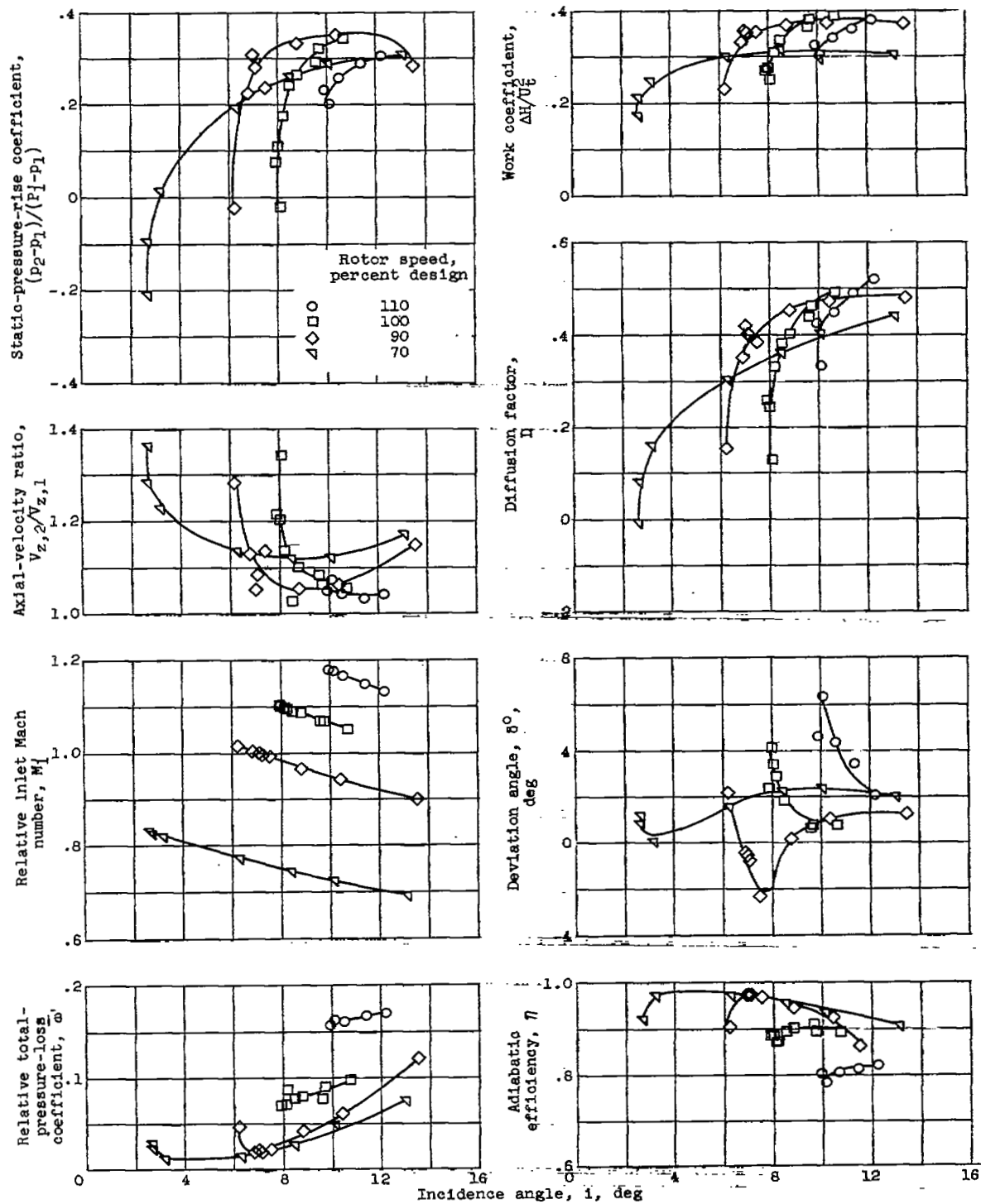


(a) Radial station A: 10 percent of passage height from outer wall.

Figure 9. - Rotor blade-element data.

4713

CA-5

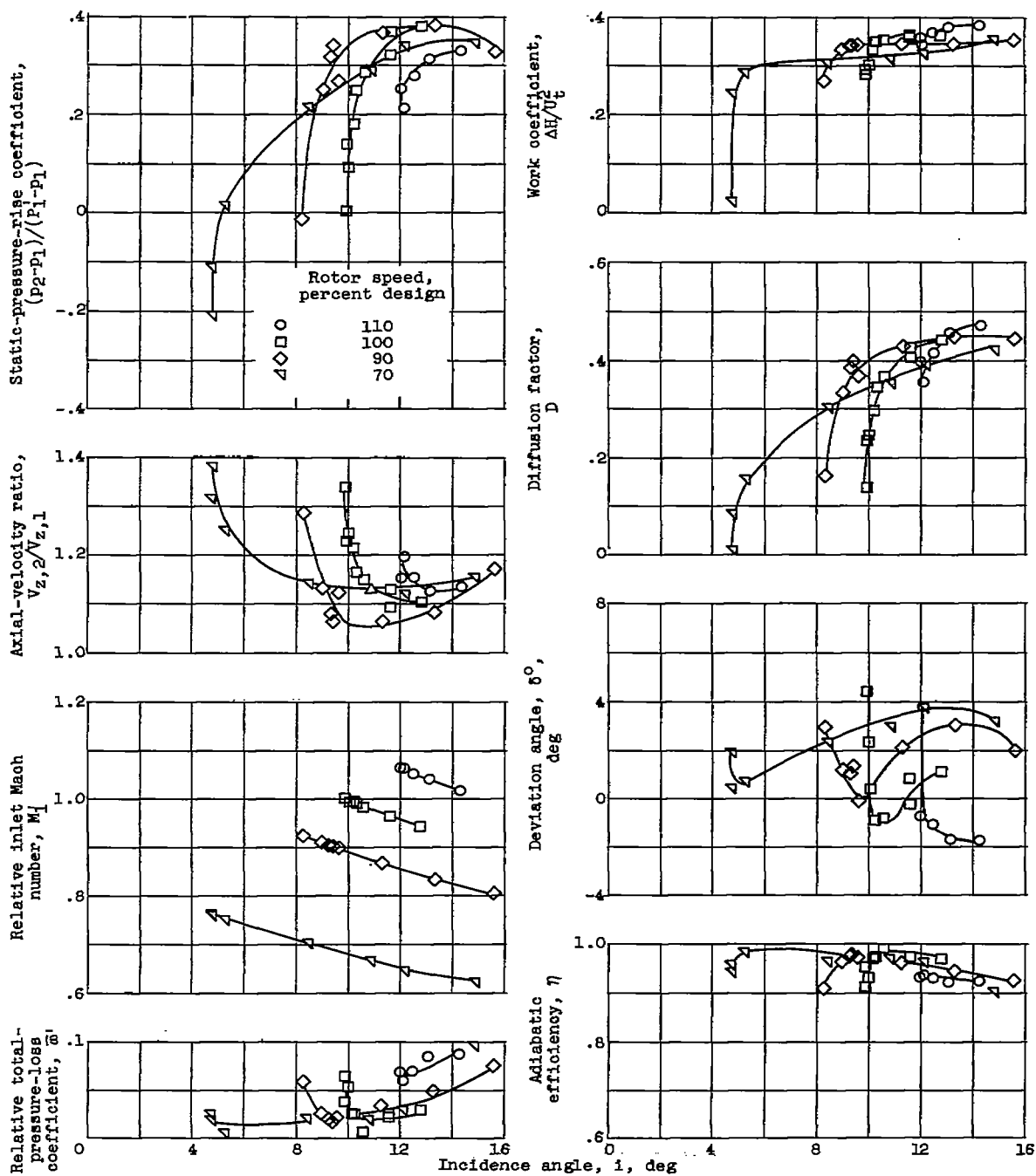


(b) Radial station B: 30 percent of passage height from outer wall.

Figure 9. - Continued. Rotor blade-element data.

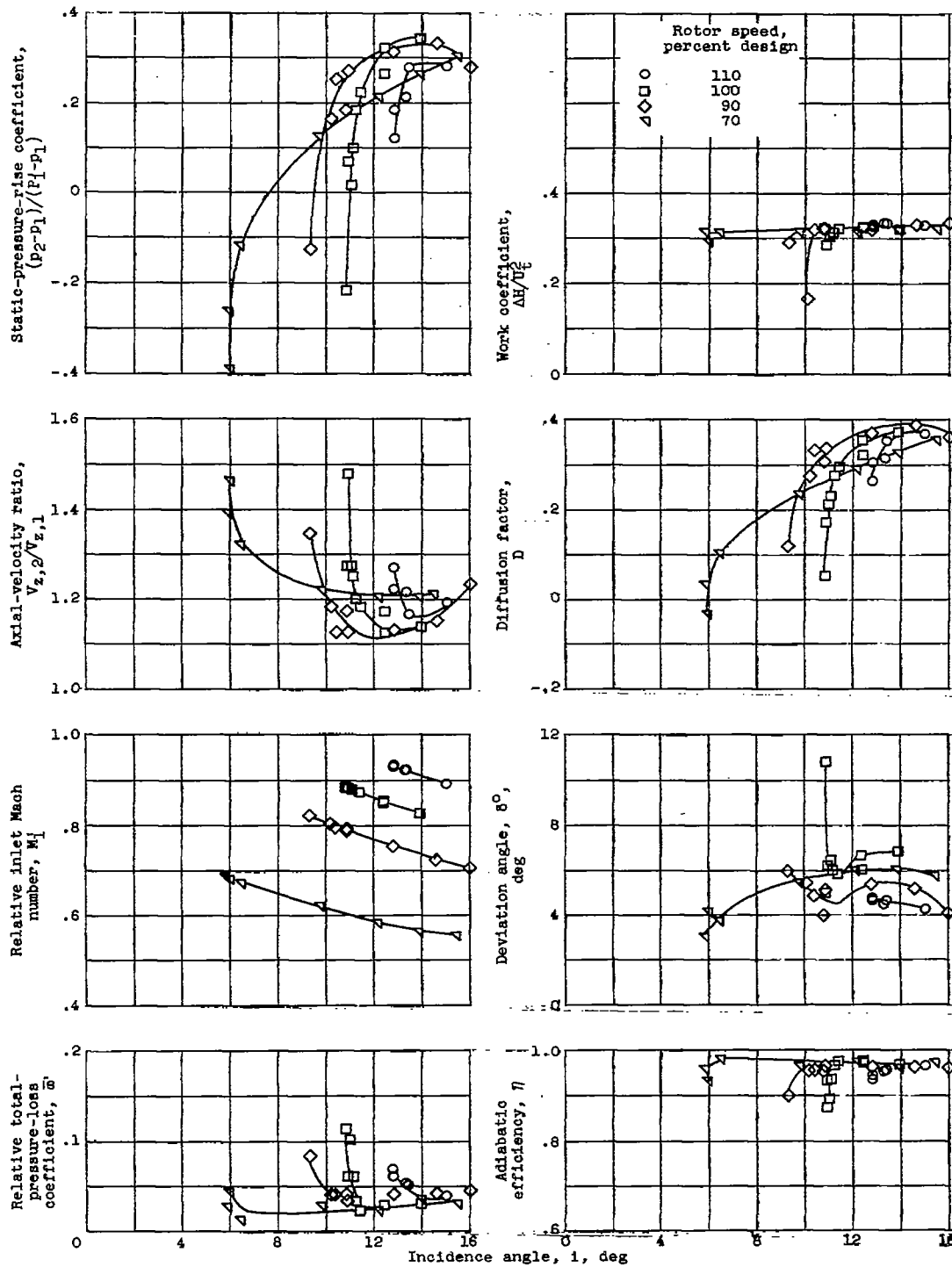
4713

CA-5 back



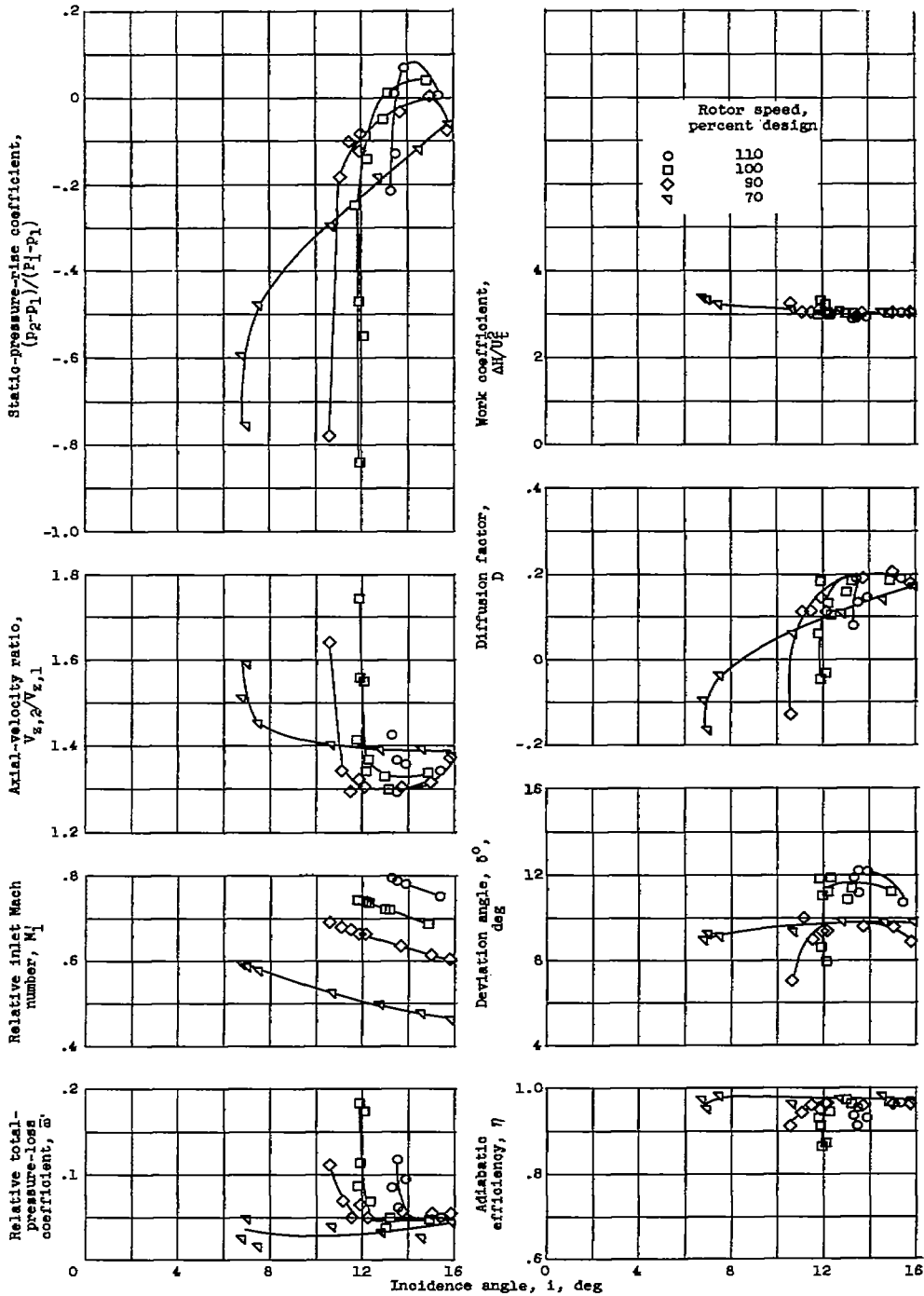
(c) Radial station C: 50 percent of passage height from outer wall.

Figure 9. - Continued. Rotor blade-element data.



(d) Radial station D: 70 percent of passage height from outer wall.

Figure 9. - Continued. Rotor blade-element data.



(e) Radial station E: 90 percent of passage height from outer wall.

Figure 9. - Concluded. Rotor blade-element data.

4713

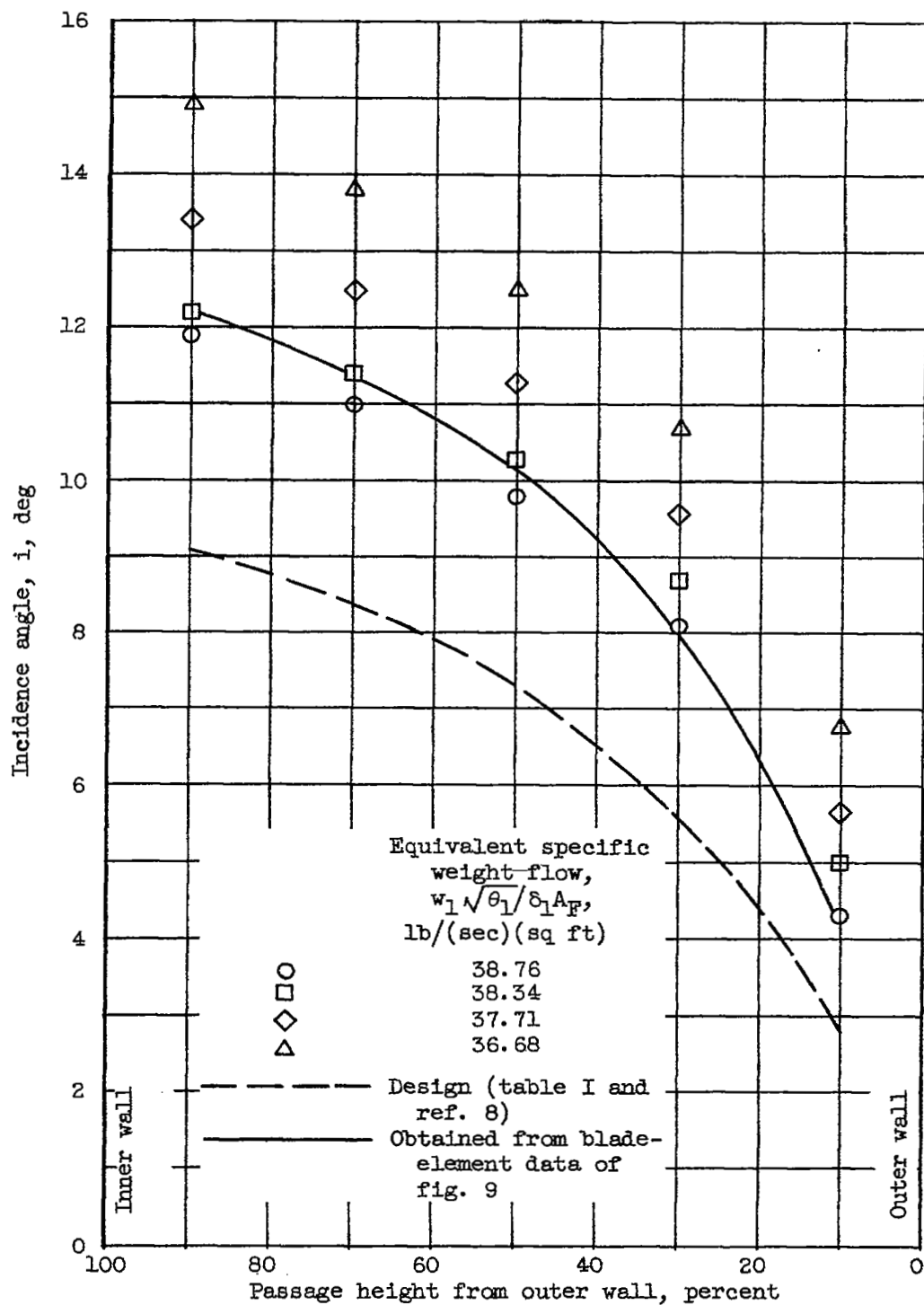


Figure 10. - Variation of incidence angle at design speed.

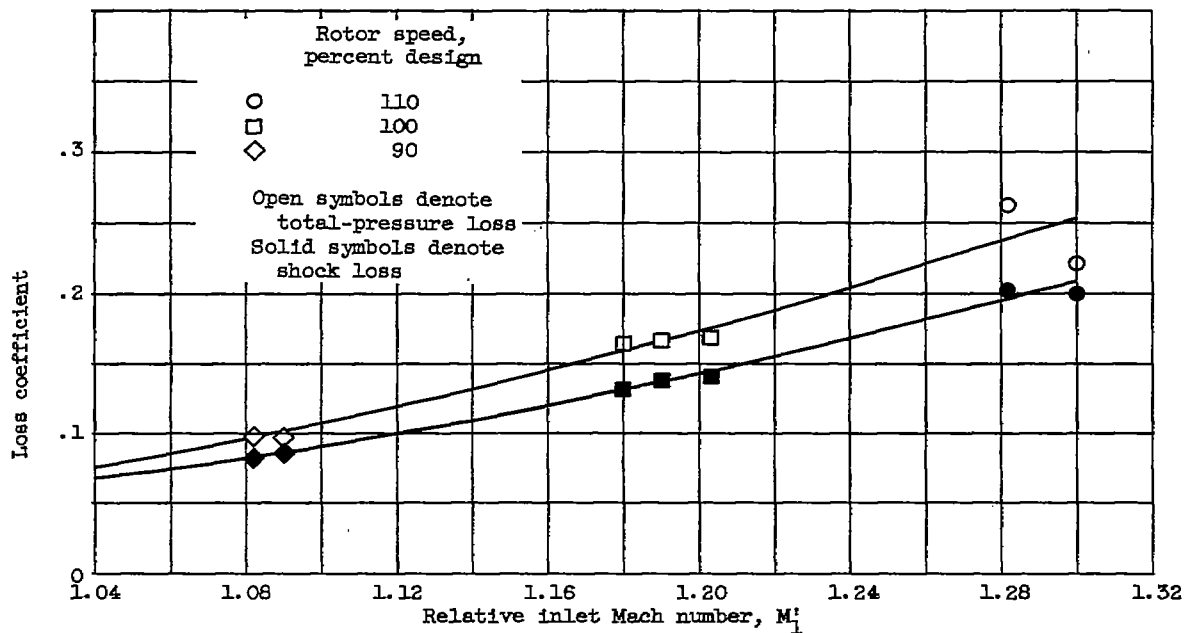



Figure 11. - Variation of rotor tip total-pressure-loss coefficient and shock-loss coefficients with inlet relative Mach number at near minimum-loss incidence angles.

4713

[Redacted]

NASA Technical Library

3 1176 01435 9195

[Faint markings]

!

[Redacted]

!

[Faint markings]